HHS Public Access

Author manuscript

Cell Rep. Author manuscript; available in PMC 2023 February 05.

Published in final edited form as:

Cell Rep. 2022 July 26; 40(4): 111066. doi:10.1016/j.celrep.2022.111066.

Reciprocal SOX2 regulation by SMAD1-SMAD3 is critical for anoikis resistance and metastasis in cancer

Zainab Shonibare[1,2], **Mehri Monavarian**[1], **Kathleen O'Connell**[2], **Diego Altomare**[3], **Abigail Shelton**[4], **Shubham Mehta**[2], **Renata Jaskula-Sztul**[5], **Rebecca Phaeton**[6], **Mark D. Starr**[7], **Regina Whitaker**[8], **Andrew Berchuck**[8], **Andrew B. Nixon**[7], **Rebecca C. Arend**[9], **Nam Y. Lee**[10], **C. Ryan Miller**[4], **Nadine Hempel**[11,12,*], **Karthikeyan Mythreye**[1,2,13,*]

[1]Department of Pathology, O'Neal Comprehensive Cancer Center, University of Alabama School of Medicine, Birmingham, AL, USA

[2]Department of Chemistry and Biochemistry, University of South Carolina, Columbia, SC 29208, USA

[3]Department of Drug Discovery and Biomedical Sciences, College of Pharmacy, University of South Carolina, Columbia, SC 29208, USA

[4]Department of Pathology, O'Neal Comprehensive Cancer Center, Comprehensive Neuroscience Center, University of Alabama School of Medicine, Birmingham, AL, USA

[5]Department of Surgery, University of Alabama School of Medicine, Birmingham, AL, USA

[6]Department of Obstetrics and Gynecology, and Microbiology and Immunology, College of Medicine, Pennsylvania State University, Hershey, PA, USA

[7]Department of Medicine and Duke Cancer Institute, Duke University Medical Center, Durham, NC, USA

[8]Department of Obstetrics and Gynecology, Duke University Medical Center, Durham, NC, USA

[9]Department of Gynecology Oncology, University of Alabama School of Medicine, Birmingham, AL, USA

[10]Department of Chemistry and Biochemistry, Department of Pharmacology, University of Arizona, Tucson, AZ 85721, USA

*Correspondence: nah158@pitt.edu (N.H.), mythreye@uab.edu (K.M.).

AUTHOR CONTRIBUTIONS

Z.S. contributed to study design, executed, and analyzed most of the experiments and wrote the paper. M.M. and K.O.C. conducted a subset of experiments. S.M. and R.J.-S. assisted in cell culture studies and neuroendocrine cell lines. D.A. conducted and analyzed microarray studies. A.S. and R.M. conducted and analyzed RNA-seq studies. M.D.S. and A.B.N. conducted and analyzed patient ascites ELISA studies. R.P., R.A., A.B., and R.W. provided patient ascites. N.Y.L. assisted in data interpretation. N.H. contributed to design and data interpretation and editing of the manuscript. K.M. conceived, conceptualized, and supervised the study, designed experiments, analyzed data, and wrote the manuscript.

DECLARATION OF INTERESTS

The authors declare no competing interests.

SUPPLEMENTAL INFORMATION

Supplemental information can be found online at https://doi.org/10.1016/j.celrep.2022.111066.

[11]Department of Pharmacology, and Obstetrics and Gynecology, College of Medicine, Pennsylvania State University, Hershey, PA, USA

[12]Department of Medicine, Division of Hematology Oncology, University of Pittsburgh, School of Medicine, Pittsburgh, PA 15213, USA

[13]Lead contact

SUMMARY

Growth factors in tumor environments are regulators of cell survival and metastasis. Here, we reveal the dichotomy between TGF-β superfamily growth factors BMP and TGF-β/activin and their downstream SMAD effectors. Gene expression profiling uncovers *SOX2* as a key contextual signaling node regulated in an opposing manner by BMP2, -4, and -9 and TGF-β and activin A to impact anchorage-independent cell survival. We find that SOX2 is repressed by BMPs, leading to a reduction in intraperitoneal tumor burden and improved survival of tumor-bearing mice. Repression of SOX2 is driven by SMAD1-dependent histone H3K27me3 recruitment and DNA methylation at *SOX2*'s promoter. Conversely, TGF-β, which is elevated in patient ascites, and activin A can promote SOX2 expression and anchorage-independent survival by SMAD3-dependent his-tone H3K4me3 recruitment. Our findings identify SOX2 as a contextual and contrastingly regulated node downstream of TGF-β members controlling anchorage-independent survival and metastasis in ovarian cancers.

Graphical abstract

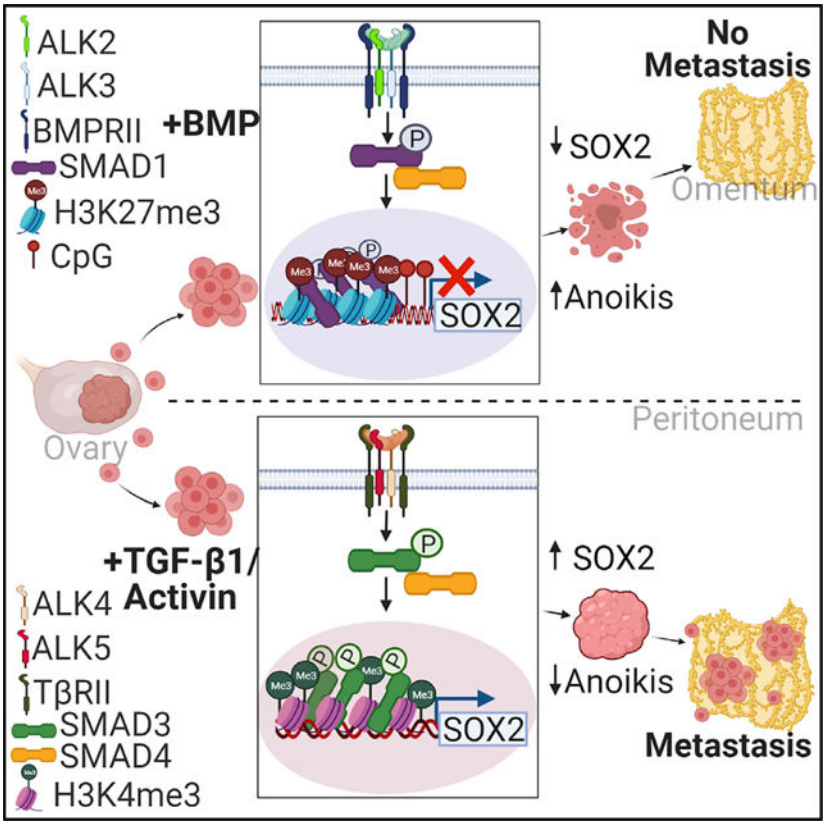

In brief

Tumor cell survival upon loss of attachment is critical for metastasis. Shonibare et al. identify SOX2 as a contextual node regulated contrastingly by BMPs and TGF-β. Regulation occurs via distinct SMAD1- and SMAD3-dependent histone recruitment and DNA methylation mechanisms influencing anchorage-independent cell survival and intraperitoneal ovarian cancer metastasis.

INTRODUCTION

Ascites accumulation in the abdomen is associated with diseases of the peritoneal cavity, with 30% related to ovarian cancer (OC). More than 90% of stages III and IV OC patients present malignant ascites, which harbor cancer cell clusters in suspension that contribute to metastasis (Huang et al., 2013). Such tumor cells exhibit anchorage-independent survival due to evasion of anchorage-independent cell death mechanisms (termed anoikis [Frisch and Francis, 1994]) in the ascites environment enriched with growth factors that can contribute to recurrence and therapy resistance (Ahmed and Stenvers, 2013; Lane et al., 2015; Monavarian et al., 2022). Thus, defining specific growth factors that promote cell survival in the ascites and conversely defining strategies that disrupt survival and promote anoikis will improve our ability to control recurrence and mortality of advanced OC patients.

The transforming growth factor β (TGF-β) family of cytokines that include TGF-βs, bone-morphogenetic proteins (BMPs/GDFs), activins, inhibins, glial-derived neurotrophic factors, and nodal have crucial roles in development and cancer (Wakefield and Hill, 2013). Cellular responses are initiated upon ligand binding to the type I and type II serine threonine kinases and type III cell surface TGF-β receptors. The types I and II receptors form ligand-dependent homomeric and heteromeric complexes (Dore et al., 1998; Ehrlich et al., 2012) to phosphorylate intracellular-receptor-regulated SMADs (R-SMADs). R-SMADs complex with the common SMAD4 and accumulate in the nucleus to regulate gene expression (Ross and Hill, 2008).

Although members of the TGF-β superfamily share similarities in the signaling events, they differ in their receptor affinities and the complexes formed. The BMP ligands (BMP2, 4, 9/*GDF2*, and BMP10) bind type I receptors: ALK1 (*ACVRL1*), ALK2 (*ACVR1*), ALK3 (*BMPR1A*), or ALK6 (*BMPR1B*), which recruit the type II receptor (BMPR2), leading to phosphorylation and nuclear translocation of the SMAD1/5/8-SMAD4 complex. BMP2 and BMP4 share a high degree of sequence identity and effectively bind ALK2, -3, and -6 receptors (Martinez-Hackert et al., 2021; Miyazono et al., 2005). BMP9 and BMP10 both have high affinity for ALK1 (David et al., 2007). However, only BMP9 can also interact with ALK2 and ALK3/6 receptors (Luo et al., 2010; Olsen et al., 2014). TGF-βs and activin, on the other hand, first bind the type II receptor (TβRII/ACTR-IIA/B), which complexes with the type I receptors ALK4 (*ACVR1B*), ALK5 (*TGFβR1*), and ALK7 (*ACVR1C*) to mediate downstream signaling via SMAD2/3 (Heldin and Moustakas, 2016). BMPs can also induce SMAD2/3 signaling via ALK3/6 (BMP-binding type I) and ALK5/7 (TGF-β-binding type I) receptors (Holtzhausen et al., 2014). Similarly, TGF-β1 can also lead to phosphorylation of SMAD1/5 via ALK2/3 and ALK5 receptors (Ramachandran et

al., 2018). SMAD1/5 activation by activin is seldom seen but has been reported (Canali et al., 2016).

In addition to cross-utilization of receptors, TGF-β/activin and BMP can both cooperate and antagonize each other (Yuan et al., 2018; Zeisberg et al., 2003; Candia et al., 1997; Ikushima et al., 2009; Ren et al., 2014). In cancer, both ligands can have tumor-suppressive and -promoting effects (David and Massagué, 2018; Singh and Morris, 2010). However, limited studies have delineated the function and relationship between TGF-β members, including BMPs (2, 4, 9, and 10), TGF-β1, and activin during metastasis. Here, we set out to delineate their relationship in a singular context of OC anchorage-independent survival that impacts metastasis, to elucidate their pathological and signaling relationship. In doing so, we identified SOX2 as a central regulated node downstream of BMP9, BMP2, BMP4, TGF-β1, and activin.

Sex-determining region Y-box 2 (SOX2), is a single-exon transcription factor with key roles in embryonic development and stem cell maintenance (Wegner, 2010; Sinclair et al., 1990). In cancer, SOX2-mediated transcriptional reprogramming is associated with a stem cell fate and tumor-initiating capacity (Bareiss et al., 2013). Although *SOX2* is an indicator of premalignant lesions and a proposed biomarker in OC (Hellner et al., 2016), it has been paradoxically linked to both poor and better outcomes (Pham et al., 2013; Wang et al., 2014; Weina and Utikal, 2014). Thus, defining its precise contextual roles and mechanisms that regulate expression is critical.

We demonstrate contextual regulation of SOX2 by TGF-β members. We find SOX2 to be a central repressed target of BMPs (9, 2, 4) leading to suppression of anchorage-independent survival and metastasis. SOX2 repression occurs through DNA and chromatin modification-based mechanisms mediated by SMAD1/5, leading to increased cell death under anchorage independence (referred to as anoikis). Conversely, TGF-β which is significantly elevated in patient ascites, and activin A increase SOX2 expression in a SMAD3-dependent manner, leading to decreased anoikis. Notably, the presence of BMPs and SMAD1 signaling can override the effects of TGF-β and activin on SOX2. Our findings implicate the use of a subset of BMPs as a therapeutic strategy and demonstrate a critical role of context-specific SOX2 regulation in controlling anchorage-independent survival and metastasis in ovarian cancer.

RESULTS

BMP2 and -9 suppress anchorage-independent survival and promote anoikis

We previously demonstrated promoter methylation of the gene for BMP9 (*GDF2*) in OC, with BMP9 increasing anoikis in a subset of cell lines (Varadaraj et al., 2015). To expand and test other BMPs, we examined BMP2 alongside BMP9 in a panel of OC cell lines. Cell lines representing a spectrum of OCs, including PA1 (ovarian teratocarcinoma), OVCA420 (serous adenocarcinoma), OVCAR3 (carcinoma high-grade serous), SKOV3 (carcinoma non-serous), and OVCA433 (serous adenocarcinoma) were grown under anchorage-independent suspension culture conditions. Treatment with BMP2 and BMP9 significantly decreased the live-to-dead cell ratio in spheroids (1.8–4.25 times decrease;

Figure 1A) with an increase in the percentage of dead cells (Figure S1A). Spheroids treated with either BMP2 or BMP9 also exhibited reduced 3D invasion capabilities (55%–67% reduction; Figure S1B). We had previously reported no effect of BMP9 on *in vitro* 2D cell growth (Varadaraj et al., 2015), and consistently, both BMP2 and BMP9 did not alter cell growth for 3 days (Figure S1C). These data indicate that both BMP2 and BMP9 promote anoikis and diminished spheroid invasion in a spectrum of OC lines.

BMP9 suppresses metastatic growth in the peritoneal cavity

Since anoikis is known to impact intraperitoneal (i.p.) OC metastasis (Cai et al., 2015; Torchiaro et al., 2016), we evaluated the effect of administering recombinant human (rh)BMP9 on peritoneal tumor growth and metastasis *in vivo*. Delivery of BMP9 was used to mimic a potential therapeutic regimen. Overall toxicity of administering BMP9 i.p. daily, examined by body weight and kidney and liver function tests, revealed no notable toxicity for up to 3 weeks (Figures S1D and S1E).

The effect of BMP9 on *in vivo* tumor growth was tested by injecting PA1 cells with either vehicle or BMP9 into the peritoneal cavity of NOD-SCID mice, followed by daily BMP9 or vehicle administration. By using bioluminescence imaging (BLI), a significant reduction in overall i.p. tumor burden over time was observed in mice receiving BMP9 compared with mice receiving vehicle (Figures 1B and 1C). Mice euthanized upon morbidity at the end of a 7-week study for PA1 cells confirmed extensive tumor burden in the omentum (Figure 1D) in the vehicle-treated group. In contrast, rhBMP9-treated mice had significantly lower omental tumor burden (Figure 1D). Similar results were observed with a second cell line, SKOV3 (Figures 1E and 1F). BMP9 treatment led to significantly lower intraperitoneal tumor growth as demonstrated by BLI in the abdomen by day 16 in the vehicle group (Figures 1E and 1F). BMP9 administration also prolonged survival in mice compared with the vehicle group (Figure 1G). Whereas all vehicle mice succumbed to disease between days 17 and 21 (Figure 1G), BMP9-treated mice survived significantly longer, for between 30 and 40 days (Figure 1G). Additionally, whereas all vehicle-treated mice had some ascites that was not measurable accurately, none of the rhBMP9-treated mice had any detectable ascites.

Histological comparison of tumors from both cell lines (PA1 and SKOV3) revealed tumor cells in large nodules in the omentum of the vehicle-treated group. In contrast, omental tumors from BMP9-treated mice consisted of significantly fewer infiltrated tumor cells (Figures 1H, 1I, and S1F). Apoptosis analysis by TUNEL staining revealed an increase in TUNEL-positive cells in tumors from BMP9-treated mice compared with vehicle-treated mice in both PA1-luc-GFP and SKOV3-luc-GFP groups (Figures 1H and 1I; 2× increase in PA1 and 14× in SKOV3). The increases in apoptosis and necrotic lesions (Figure S1G) found in tumors from BMP9-treated mice was noted widely. ELISA analysis confirmed elevated BMP9 in the plasma from mice, verifying their presence in circulation (Figure S1H). Thus, administration of (rh) BMP9 along with i.p.-injected tumor cells *in vivo*, which mimics the shedding of tumor cells into the peritoneal cavity during metastasis, suppresses intraperitoneal tumor spread and growth and prolongs survival of mice in two OC i.p.-xenograft models.

SOX2 is a repressed transcriptional target of BMP2, -4, and -9, but not BMP10, in cancer

To identify critical factors regulating anoikis in response to BMP, we compared the transcription profile of 48,226 genes in PA1 cells cultured under anchorage-independent growth conditions treated with either BMP9 or vehicle control (Figures 2A and Figure S2A). We found 543 differentially expressed genes using a 2-fold change criterion ($p < 0.05$, GEO: GSE185924), which were further divided into upregulated (n = 333) and downregulated genes (n = 210) in response to BMP9 (Figure S2A and Table S4). REACTOME analysis identified 18 pathways significantly altered, including BMP and TGF-β signaling, and transcriptional regulation of pluripotency-associated genes (Figure S2B and Table S4). Notably, examination of the 30 top altered genes (15-up and 15-down) revealed *SOX2*, *IGFBP5*, and *HTR1D* as the most repressed genes in BMP9-treated cells (12.37- to 20-fold change in gene expression; Figure 2B). Additionally, among the top 30 altered genes, 28 were linked to *SOX2* through PubMed searches (Card et al., 2008; Wang et al., 2015; Lach-mann et al., 2010; Si et al., 2019; Lim et al., 2007; Bani-Yaghoub et al., 2006; Ehlers and Todd, 2017; Kelberman et al., 2006; Seki, 2018; Acanda de la Rocha et al., 2016) and the GENECARD human gene database.

In OC cell lines, SOX2 expression at baseline is variable, with PA1 cells expressing the highest relative mRNA and protein level of SOX2, followed by OVCAR3 and SKOV3 (Figure 2C). Using this panel as a guide, we validated *SOX2* downregulation by BMP9 via qRT-PCR in anchorage-independent conditions (Figure S2C). BMP9 did not have any significant effect on two other developmental transcription factors, *OCT4* or *NANOG* (Figure S2D). Reduction in SOX2 expression by BMP9 was significant in several cell lines even under attached growth conditions, including in OVCAR3 and SKOV3, which express detectable RNA and protein levels of SOX2 (Figures 2C and 2D). Furthermore, downregulation of SOX2 was mediated by two additional BMP ligands, BMP2 and BMP4 (Figure 2E), with decreases at the protein (Figure 2F) and RNA levels in both PA1 and OVCAR3 cells (Figure 2G). BMP4 also promotes anoikis, as treatment with BMP4 significantly decreased the live-to-dead cell ratio in PA1 cells under anchorage independence (1.9× Figure S2E). However, BMP10, which exhibits the highest sequence homology to BMP9 (Tillet and Bailly, 2014), did not alter SOX2 (Figure 2E), or anoikis (Figure S2F).

BMP9-mediated SOX2 repression also occurred in xeno graft tumors, as IHC analysis of SOX2 and qRT-PCR analysis revealed an overall reduction in SOX2 levels in tumors from BMP9-treated mice compared with vehicle control-treated mice (Figures 2H and S2G). Importantly, we found that patient ascites-derived tumor cells EOC15 and AF68 express *SOX2* under anchorage-independent conditions, which was downregulated by BMP9 treatment as well (Figure 2I). In addition to OC, several other cancer types are known to express SOX2, including lung (Ochieng et al., 2014), pancreatic neuroendocrine, and bronchial carcinoid tumor (Akiyama et al., 2016). We found that BMP2 and BMP9 treatment downregulated SOX2 expression in A549 (lung cancer), BON-1 (P-NET), and H727 (bronchial carcinoid tumor) cells as well (Figure 2J).

Since we observed that BMPs induce anoikis in both high-SOX2-expressing cell lines (PA1, OVCAR3, SKOV3) and low-SOX2-expressing cell lines (Figures 1A and 2C), we tested whether SOX2 levels were altered under anchorage independence, to potentially

explain why BMP increased anoikis in endogenously low-SOX2-expressing cells. Indeed, OVCAR4, OVCA420, and OVCA433 cells (low SOX2 expression) significantly upregulate *SOX2* expression under anchorage independence (Figure 2K). These increases in *SOX2* were effectively suppressed by both BMP2 and BMP9 (Figure 2L). We noted that changes in SOX2 under anchorage independence were not restricted to low-SOX2 cell lines but were also measurable in cell lines with higher baseline levels, including OVCAR3 and PA1 (Figures S3A and S3B), which were also suppressed by BMPs (Figure S2C). All together, these results indicate that BMP2, -4, and -9 can downregulate SOX2 in multiple cancer types either when endogenous levels are high or when SOX2 expression is induced in response to anchorage-independent growth or during *in vivo* tumor progression.

Rapid transcriptional downregulation of SOX2 is sufficient for anoikis

Kinetics and dose-response studies reveal dose-dependent repression of SOX2 by both BMP2 and BMP9, with BMP9 being pronounced at lower doses compared with BMP2 (Figure 3A). SOX2 protein repression began within 6 h post-treatment and by 2 h at the mRNA level in both PA1 (Figure 3B) and OVCAR3 cells (Figure 3C). We also found that both BMP2 and BMP9 significantly reduce luciferase activity of a 1-kb *SOX2* promoter reporter (Yeh et al., 2018) (Figure 3D). Expressing SOX2 from a heterologous promoter (CMV) prevented BMP2- and BMP9-mediated decreases in SOX2 in SKOV3 cells (Figure 3E). Similar overexpression of SOX2 from a different heterologous promoter (EF1a) in PA1 cells that express high levels of endogenous SOX2, was able to suppress the decrease of SOX2 by BMP2 and BMP9 (Figure 3F), accounting for both the endogenous and the heterologous EF1a-driven SOX2. Overexpression of SOX2 from a heterologous promoter resulted in suppressing anoikis (increased anchorage-independent survival) and generated compact spheroids compared with control cells (Figure 3G; CMV-SOX2). BMPs, however, had no significant effect on anoikis in cells overexpressing SOX2 from the CMV promoter (CMV-SOX2; Figure 3H) compared with that in control cells (SKOV3-CMV-control; Figure 3H). These data demonstrate that SOX2 is necessary for survival under anchorage independence by inhibiting anoikis and is a major transcriptionally repressed target of BMP for anoikis.

Patient ascites are low in BMP9 but high in TGF-β, which upregulates SOX2 and promotes anchorage-independent survival by suppressing anoikis

To evaluate the levels of BMPs and other TGF-β members, particularly (TGF-β1/2), in OC patient ascites, an environment bearing tumor cells under anchorage independence, we used ligand-specific ELISAs. BMP9 could not be detected in patient ascites irrespective of disease stage (Figure 4A). In contrast, significantly higher levels of TGF-β1 (3800–52,348 pg/mL) and TGF-β2 (64–4,259 pg/mL) were present, with TGF-β1 being an order magnitude higher than TGF-β2 (Figure 4A). On the basis of these observations, we tested the effect of TGF-β1 on SOX2. In contrast to BMP2 and -9, TGF-β1 increased SOX2 protein and mRNA expression under both attached (Figures 4B–4D) and anchorage-independent conditions (Figure S4A). Activin, another TGF-β member, also increased SOX2 levels, like TGF-β1 (Figure 4B). In a corollary fashion, live-dead analysis of anchorage-independent spheroids treated with TGF-β1 increased the live/dead ratio in OC cells (PA1, OVCA420, and OVCAR3; Figure 4E), with spheroids treated with activin A demonstrating

a similar trend in reduction of cell death under anchorage independence (Figure S4B). Luciferase activity of the 1-kb *SOX2* promoter reporter construct (Yeh et al., 2018) was increased in response to TGF-β1 treatment (Figure 4F) and activin A (Figure S4C) as well.

Since BMP9 and TGF- β1 have opposing effects on SOX2, and TGF-β1 is present at high levels in the ascites of patients (Figure 4A), we evaluated whether TGF-β1 or activin A would override the effects of BMP9 on SOX2 repression. Equimolar amounts of BMP9 or TGF-β1 either decreased or increased SOX2 respectively, whereas the combination treatment led to a 70% reduction in SOX2 (Figure 4G). Similar lowering of SOX2 was observed when activin A and BMP9 were combined (Figure S4D). These findings on the differential effects of BMP and TGF-β on SOX2 and anoikis (Figures 3 and 4) point to SOX2 as an important node determining anchorage-independent survival in response to TGF-β ligands and implicate BMP9 as a feasible way to override the effects of TGF-β on SOX2.

SOX2 levels are differentially regulated by ALK2, ALK3, and ALK5

Our findings on the differential effects of TGF-β ligands and the difference in the extents of SOX2 repression between BMP ligand isoforms (BMP9>>BMP2; Figures 3 and 4B), prompted us to delineate receptor and SMAD signaling involvement downstream of these ligands. We used a panel of small-molecule inhibitors to the different type I (ALK) receptors; Dorsomorphin (DM, ALK2/3/6 [Hao et al., 2008]); SB431542 (ALK4/5/7 [Inman et al., 2002]); ML347, (ALK1/2 [Engers et al., 2013]), and LDN193189 (ALK2/3 [Boergermann et al., 2010]). Whereas BMP9 repressed SOX2 both at the protein and mRNA level in vehicle-control cells (Figure 5A in PA1; Figure S5A for OVCAR3), inhibiting ALK2/3/6 resulted in 34.3% recovery in SOX2 levels in the presence of BMP9 (Figure 5A, DM lanes). Inhibiting ALK4/5/7 did not significantly alter the extent of SOX2 repression by BMP (Figure 5A, SB lanes). Similarly, inhibiting ALK2/3/6 in BMP2-treated cells resulted in a 23% recovery in SOX2 repression (Figure 5B, DM lanes, and Figure S5B). Again, inhibiting ALK4/5/7 did not alter the extent of SOX2 repression by BMP2 (Figure 5B, SB lanes). Phosphorylated SMAD1 (pSMAD1) in response to BMP2 and -9 was repressed by DM (ALK2,3,6 inhibition), with no effects observed upon co-treatment with SB431542 (ALK4/5/7 inhibition). Interestingly, inhibiting ALK1/2 with ML347 increased baseline SOX2 levels even in the absence of exogenous ligand (Figure 5C, ML347 lane 4) and abrogated the ability of BMP9 to repress SOX2 at both protein and mRNA levels in PA1 (Figure 5C, ML347 + BMP9 compared with BMP9 lanes) and OVCAR3 cells (Figure S5C). Compared with BMP9, ALK1/2 inhibition only partially prevented BMP2-mediated SOX2 repression (72% recovery; Figure 5C, ML347 + BMP2 compared with BMP2 lanes). BMP9-induced phosphorylation of SMAD1 was completely suppressed with ML347 (Figure 5C, ML347 lanes, and Figure S5C), with only partial (40%) suppression of BMP2-induced SMAD1 phosphorylation (Figure 5C). Similarly, inhibition of ALK2,3 using LDN193189 increased SOX2 protein levels at baseline even in the absence of exogenous ligand (3×; Figure 5C) and blocked both BMP2's and BMP9's ability to repress SOX2 (Figure 5C). Full inhibition of BMP2- and BMP9-induced SMAD1/5 phosphorylation was also observed (Figure 5C, LDN lanes, and Figure S5C, OVCAR3 cells). All together, these data demonstrate a strong preference for ALK2 in BMP9-dependent SOX2 repression at both the

protein and RNA levels and a combination of ALK2 and ALK3 in BMP2-dependent SOX2 repression.

To confirm specific roles of ALK2 and ALK3 receptors in SOX2 repression, constitutively active kinases ALK2 or ALK3 (HA-ALK2QD and HA-ALK3QD) (Imamura et al., 1997) were expressed in PA1 and OVCAR3 cells. Activating ALK2 kinase (ALK2QD) decreased SOX2 even in the absence of exogenous BMP ligand (69% reduction in PA1 and 90% in OVCAR3; Figures 5D and 5E). In the presence of ligand (BMP2, BMP9), ALK2QD-mediated SOX2 repression was further enhanced (Figures 5D and 5E). The effect of activating ALK3 (ALK3QD) was modest compared with ALK2QD and was cell line dependent. ALK3QD did not reduce SOX2 in the absence of exogenous ligand in PA1 cells but was able to reduce SOX2 levels by 65% in OVCAR3 cells in the absence of exogenous ligand (Figures 5D and 5E). The presence of ligand (BMP2, BMP9) only slightly enhanced SOX2 repression in both cell lines with ALK3QD (Figures 5D and 5E). These findings demonstrate a requirement for both ALK2 and ALK3, with ALK2 being critical for maximum SOX2 downregulation based on ligand-independent effects and enhancement of the effects of both BMP9 and BMP2.

Since both TGF-β1/2, and activin predominantly utilize ALK4/5/7 for phosphorylating SMAD2/3, we evaluated the effect of blocking their kinase activity using SB431542. We found that SB431542 suppressed TGF-β1-induced SOX2 increases (Figures 5F and 5G). These studies together implicate different ALK receptors: ALK2 and ALK3 in SOX2 repression and ALK4 and ALK5 in increasing SOX2 expression.

SMAD1 and SMAD3 differentially regulate SOX2 and occupy the *SOX2* promoter in response to BMP9 and TGF-β, respectively

SMAD1 phosphorylation is a primary response to ALK2 and ALK3 kinases (Heldin and Moustakas, 2016) that regulate SOX2 levels downstream of BMP (Figure 5). We previously reported a SMAD1-signaling preference for BMP9 (Varadaraj et al., 2015). Hence, we tested a direct role for SMAD1 in SOX2 repression by using pooled shRNAs to SMAD1 (shSMAD1). Reducing SMAD1 significantly decreased the ability of BMP2 and BMP9 to reduce SOX2 levels compared with control shRNA cells (shNTC) by 30–44% (Figure 6A). Since ALK5, downstream of TGF-β signaling (Figures 5F and 5G), primarily phosphorylates SMAD2/3 (Heldin and Moustakas, 2016), we silenced SMAD3 using pooled siRNAs (Figure 6B). TGF-β increased SOX2 levels in control (siScr) cells (Figure 6B) but was unable to increase SOX2 in siSMAD3 cells (Figure 6B). Strikingly, siRNA to SMAD3 also lowered SOX2 levels at the baseline even in the absence of exogenous ligands (Figure 6B), indicating direct roles for SMAD3 in SOX2 upregulation. We also observed a compensatory increase in pSMAD1 upon lowering of SMAD3 (Figure 6B) that correlated with lower SOX2 levels even in the presence of TGF-β1 (Figure 6B).

In silico analysis revealed several SMAD1- and SMAD3-binding motifs (GG(C/A)GCC and GTCT/AGAC, respectively) within 2 kb of the transcriptional start site for *SOX2* (TSS; Figure 6C) (Martin-Malpartida et al., 2017). Chromatin immunoprecipitation (ChIP) was used to assess the binding of SMADs to these sites. The promoter contains four SMAD1 and two SMAD3 motifs. However, due to several “CG” clusters (CpG islands), we designed

primers, flanking regions immediately outside the CpG islands with additional sites within 2 kb of the TSS (Figure 6C). Primers flanking SMAD1-binding elements (p1, p2, p5, p6) and primers flanking SMAD3-binding elements (p1, p3, p4, and p5) were used, with p1 and p5 having both SMAD1- and SMAD3-binding elements, and p6 located closest to the TSS (Figure 6C). BMP9 treatment led to a significant enrichment of SMAD1 binding at two sites: p1 and p6 (Figure 6D); p2 and p5 had modest SMAD1 enrichment but were not consistent in our independent biological experimental trials and, hence, are not shown here. TGF-β1 treatment led to consistent SMAD3 enrichment at p1, p3, p4, and p5 (Figure 6E). Due to the proximity of p6 to a SMAD3-binding element, we also tested and found SMAD3 enrichment at p6 as well in response to TGF-β1 treatment (Figure 6E). These sites were also tested for response to activin A and were similarly found to be occupied by SMAD3 (Figure S6). These data together indicate enrichment of SMAD1 and SMAD3 to *SOX2*'s promoter and upstream regions in response to BMP9, TGF-β1, and activin A, respectively, with one site occupied by both SMAD1 and SMAD3 and other uniquely occupied regions.

Epigenetic regulation of SOX2 is mediated by SMAD-dependent methylated histone occupancy and promoter DNA methylation

Gene repression and activation by SMADs frequently require additional proteins and chromatin modification (Hill, 2016). Hence, we evaluated whether protein degradation was required for BMP9-induced SOX2 repression. We found no effect of MG132, an inhibitor of proteasomal degradation, on BMP's ability to repress SOX2 (Figure S7A). However, histone H3K27me3 was significantly enriched on the *SOX2* promoter in response to BMP9 treatment (Figure 6F). This enrichment was SMAD1-signaling dependent, as H3K27me3 occupancy was significantly reduced in the presence of LDN193189 (ALK/SMAD1 inhibitor; Figure 6F). Notably, lowering global histone H3K27me3 in PA1, SKOV3, and OVCAR3 cells by using GSK126, an inhibitor to *EZH2*, (McCabe et al., 2012) (Figure S7B) abrogated *SOX2* repression by BMP9 in multiple cell lines (Figures 6G and S7C). These data demonstrate a role for H3K27me3 in transcriptional repression of *SOX2* downstream of BMP9 signaling.

TGF-β1 treatment, conversely, led to enrichment of H3K4me3 at multiple SMAD3 motifs (Figure 6H; p1, p3, p4, p5, p6). This enrichment was SMAD3 dependent, as H3K4me3 enrichment was abrogated by SB431542 treatment (Figure 6H). These regions are consistent with ENCODE analysis in HeLa and A549 cell lines (Figure 6C) that identified highest H3K27me3 peaks at p5 and p6, the same regions where we found SMAD1 enrichment in response to BMP9 (Figure 6D); p1 exhibited a high peak of H3K4me3, the same SMAD3-occupied region in response to TGF-β1. Our findings suggest that SMAD1 signaling and occupancy lead to an increase in histone H3K27me3, and conversely, SMAD3 signaling and occupancy lead to an increase in histone H3K4me3 at *SOX2*'s promoter and regulatory regions.

Due to the presence of CpG islands within 10 bp of the p6 primer sites, (Figure 6C), we evaluated DNA methylation in response to BMP9. Methylation-specific qPCR in response to BMP9 revealed a 2.5× increases in *SOX2* promoter methylation compared with control cells (Figure 6I). The DNA methyltransferase (DNMT) inhibitor 5′-azacytidine (5′-Aza) (Yang et

al., 2017), abrogated BMP9-induced *SOX2* promoter methylation (Figure 6I) and in parallel suppressed *SOX2* mRNA downregulation by BMP9 (Figure 6J). Interestingly, we noted a minimal effect on *SOX2* promoter methylation in PA1 cells treated with 5′-Aza alone (Figure 6I). However, compared with PA1 cells, which express high *SOX2* (Figure 2C), cells with lower baseline levels of *SOX2* such as SKOV3 (Figure 2C) suppressed *SOX2* promoter methylation significantly upon 5′-Aza treatment (Figure S7D), with a concomitant increase in *SOX2* mRNA (Figure S7E). 5′-Aza also repressed BMP9-induced *SOX2* transcriptional repression in SKOV3 cells in a similar manner to that in PA1 cells (Figure 6K). These findings confirm robust regulation of the *SOX2* locus by methylation in different cell lines and indicate that DNA methylation along with SMAD1-dependent H3K27me3 recruitment can drive SOX2 repression.

SOX2 repression leads to genome-wide changes in key transcriptional factors and cell death pathways under anchorage independence

High SOX2 is associated with a poor prognosis for OC patients (Zhang et al., 2012), and reducing SOX2 expression transiently using pooled siRNAs (siSOX2; Figure 7A) or alternatively stably using shRNA (shSOX2; Figure 7B) resulted in increased cell death under anchorage independence (anoikis) compared with control cells (Figures 7A and 7B). In both si*SOX2* and sh*SOX2* cells, spheroids appeared disaggregated and less compact compared with their respective controls (Figures 7A and 7B). The requirement of SOX2 for anchorage-independent survival led us to explore genes and pathways impacted by *SOX2* specifically under anchorage independence. Genome-wide gene expression profiles of si*SOX2* and siNTC (non-targeting control) PA1 cells were compared using RNA-sequencing from cells under anchorage independence. Our analysis revealed 59 differentially expressed genes (DEGs) between siNTC and si*SOX2* cells ($p < 0.05$; Figure 7C and Table S5), with 24 of these downregulated and 35 upregulated in siSOX2 cells compared with control (Figure 7C and Table S5). Of the total 59 DEGs, 21 of them including *SOX2* also changed their expression levels in response to BMP9 from our microarray analysis (Figures 7D and S8A). A closer analysis of the 20 genes for *SOX2*-binding motifs within 1 kb of the transcription start sites using LASAGNA-Search, revealed that 17 of 20 of the common DEGs presented one or more *SOX2*-binding motifs (Figure S8B). Downregulated DEGs had previously been implicated in processes relevant to cell adhesion (*POSTN* [Soikkeli et al., 2010]) and metastasis (*TRIM22* [Ji et al., 2021]). Gene set enrichment analysis of the differentially expressed genes from the RNA-seq data revealed enrichment of eight Hallmark gene sets based on a FDR value < 25% and included “apoptosis,” “TGF-β signaling,” and “epithelial-mesenchymal transition” in si*SOX2* cells (Figure 7E) and, interestingly, “interferon alpha response” and “interferon gamma response” in the control siNTC cells (Figure 7F). Upregulation of several genes from the apoptosis pathway, including *BMF*, *BCL2L11*, and *BID* (Figure 7E) were confirmed to be upregulated in si*SOX2* cells under anchorage independence (Figure S8C). We also analyzed genes from the TGF-β signaling pathway and identified *ACVR1* (ALK2) as one of the upregulated genes upon silencing *SOX2* (Figure S8C). Additional validated genes from the RNA seq analysis included *TRIM22*, *CD47*, and *CD74* genes from the interferon alpha and gamma response pathways in control (siNTC) cells (Figures S8C and S8D). We found *TRIM22* to be downregulated in si*SOX2* cells (Figure S8C), whereas CD47 and CD74 were upregulated in si*SOX2* cells

to different extents (Figure S8D). Taken together, these findings establish a role for *SOX2* silencing in promoting apoptosis under anchorage independence with alterations to key transcriptional and epigenetic regulators and adhesion molecules for tumor cell survival.

DISCUSSION

We provide an in-depth analysis of TGF-β family members in anchorage-independent survival and OC transcoelomic metastasis by delineating distinct effects of the TGF-β, BMP, and activin subfamilies. We previously observed a role for BMP9 (*GDF2*) in anoikis (Varadaraj et al., 2015). Here, we expand the effects of BMP9 to BMP2 and BMP4. BMP9 administration at the time of intraperitoneal tumor cell injection into mice, to mimic the shedding of tumor cell from the primary tumor, reduced transcoelomic metastasis and prolonged overall survival from disease. BMP9 also decreased spheroid invasion, which could be a result of reduced viable cells in the spheroids. Our findings alongside prior studies on the impact of BMP9 on normalizing tumor blood vessels (Viallard et al., 2020) suggest potential dual effects of the anti-tumor properties of BMP9 on the vasculature likely via the endothelial-specific TGF-β receptor *ACVRL1* (Scharpfenecker et al., 2007), and an anoikis effect on epithelial cells via ALK2,3, as seen here. Thus, therapeutic strategies that use BMP9 mimetics along with anti-angiogenics should be further investigated.

We found SOX2 at the epicenter, driving the differential effects of BMPs and TGF-β on anoikis. Although both BMP2 and BMP4 also increase anoikis and repress SOX2, BMP9 was more potent. It is possible that BMP2 may involve additional or alternate mediators besides SOX2. BMP10 had limited effects on epithelial cell anoikis, contrasting with BMP9. This may be explained by the ability of BMP9 to utilize ALK2 (Luo et al., 2010; Olsen et al., 2014). Consistent with this receptor specificity hypothesis and model, BMP10 failed to activate SMAD1/5 (Varadaraj et al., 2015), repress SOX2, and impact anoikis. Probing the receptor mechanisms revealed that ALK2/ALK3-induced phosphorylation of SMAD1 is critical for SOX2 repression. A more robust requirement of ALK2 than ALK3 was observed, which could account for higher sensitivity to BMP9 than BMP2.

Although BMP9 strongly enhanced anoikis (Varadaraj et al., 2015), it had no negative effects on attached cells *in vitro*. Both BMP2 and BMP9 have been shown to act as tumor suppressors in cancers including, but not limited to, breast (Ren et al., 2014) and prostate (Ye et al., 2008), with prior conflicting studies in OC indicating increased tumor growth in subcutaneous models (Peng et al., 2016) that do not incorporate intraperitoneal cancer spread.

A key finding here is the divergent role of TGF-β members on anoikis and SOX2. This is of clinical relevance, as patient ascites are highly enriched in TGF-β1 but not in BMP9, suggesting that OC cells are primarily exposed to TGF-β1 that stimulates SOX2 and suppresses anoikis. TGF-β can also regulate epithelial to mesenchymal transition (EMT) via SMAD3, which has been associated with anoikis resistance (Cao et al., 2016; Frisch et al., 2013) and spheroid invasion (Naber et al., 2011). Our findings are consistent with studies on inhibition of TGF-β1 signaling and reduced peritoneal tumor growth in OC (Yamamura et al., 2012; Zhang et al., 2018). With accumulating preclinical and clinical evidence on

TGF-β1 and activins as a therapeutic target in OC (Tao et al., 2019), these findings highlight an important mechanism of their pro-metastatic roles through SOX2 and anoikis resistance.

Since TGF-β1 receptor dependencies are key in the regulation of SOX2 by TGF-β family members, alterations in receptor expression could be an important tipping point in determining the balance between SMAD1 and SMAD3 signaling, leading to SOX2 downregulation or upregulation. TGF-β members, particularly TGF-β1, can also lead to phosphorylation of SMAD1/5 via ALK2/3 and ALK5 receptors (Ramachandran et al., 2018; Liu et al., 2009). However, we found that SMAD3 knockdown was sufficient to abrogate TGF-β1-mediated increases in SOX2. The compensatory increase in pSMAD1 levels that correlated with lowered SOX2 suggest that shifting the balance between SMAD1 activation and SMAD3 activation, regardless of the upstream ALK involved, could potentially tip the effect of exogenous TGF-β from increasing SOX2 to suppressing SOX2.

In ligand combination studies of TGF-β1/activin with BMP9, BMP9 could override TGF-β1/activin to downregulate SOX2. Future in-depth experiments could inform BMP9 therapeutic regimens. In a contrasting but conceptually consistent scenario, high levels of BMP antagonists such as gremlin have been reported in cancer (Neckmann et al., 2019), which might explain the loss of BMP responsiveness and tumor-suppressive function sometimes seen in OC.

The importance of our finding that SOX2 is a centrally regulated target should be emphasized, given that SOX2 is a pioneer transcription factor (Soufi et al., 2012) and can predict survival and prognosis in multiple cancers (Zhang et al., 2012; Belotte et al., 2015; Bååth et al., 2020; Sun et al., 2013; Sholl et al., 2010). Several epigenetic mechanisms can regulate *SOX2* (Alonso et al., 2011), and likely, these are exploited by the SMADs. Both increased *SOX2* promoter methylation at the CpG islands and H3K27me3/H3K4me3 enrichment occurred in a SMAD-signaling-dependent manner. H3K27me3 and H3K4me3 enrichment occurred in the same regions as SMAD1 and SMAD3 in response to BMP9 and TGF-β1 respectively, and depended on SMAD activation/phosphorylation. The contribution of DNA methylation in response to BMP9 in conjunction with H3K27me3 is a likely explanation for the high degree of SOX2 repression observed in response to BMP9.

Overall, our findings suggest that both intrinsic cellular states and the growth factor environment strongly influence SOX2, providing information on the effects of changing the balance in growth factors in the ovarian cancer ascites environment, which may inform therapeutic targeting of these pathways in ovarian cancer.

Limitations of the study

We show that BMP9 can override effects of TGF-β1 and activin on SOX2. However, recombinant proteins were used and may not fully recapitulate activities *in vivo*, and future studies will need to evaluate these interactions in depth. Although we demonstrate increased histone deposition on *SOX2*'s promoter in response to SMAD activation, direct physical SMAD-histone interactions at the promoter were not established.

STAR★METHODS

RESOURCE AVAILABILITY

Lead contact—Further information and requests for resources and reagents should be directed to and will be fulfilled by the lead contact, Mythreye Karthikeyan (mythreye@uab.edu).

Materials availability—Cell lines generated in this study are available from the lead contact upon request.

Data and code availability

- The Microarray CEL files and RNA-seq data have been deposited in the NCBI Gene Expression Omnibus (GEO) database and are publicly available as of the date of publication. Accession numbers are listed in the key resources table.
- This paper does not report any original code.
- Any additional information required to reanalyze the data reported in this paper is available from the lead contact upon request.

EXPERIMENTAL MODEL AND SUBJECT DETAILS

Mice—All animal studies were performed in accordance with the Institutional Animal Care and Use Committee at the University of Alabama Birmingham. Female SCID mice (key resources table) at 5–7 weeks of age were housed under pathogen-free conditions at the Animal Research Facility at UAB. 1.5×10^6 GFP-luciferase SK-OV3 cells or 3×10^6 GFP-luciferase expressing PA1 cells were intraperitoneally injected. Mice were monitored daily, with girth and weight measurement taken twice a week. Tumor progression was tracked weekly using the IVIS Lumina III *In vivo* Imaging System (Caliper Life Sciences, MA) at UAB's Small Animal Imaging Facility. rhBMP9 was administered at the time of tumor cell injection followed by daily intraperitoneal (i.p.) injections of 1 mg/mL in 4mM HCl + PBS + DI water (Vehicle), to achieve a final 5 mg/kg dose. For metastasis and tumor growth analysis, mice were euthanized between 21–50 days depending on the cell line. At necropsy, ascites, if present, were collected and volumes measured when possible, tumor weights in the omentum and other organs were recorded and collected when possible. For survival studies, mice that reached end-point criteria, including continued weight loss, respiratory trouble and permanent recumbency were euthanized. For microscopic analysis of tissues, formalin-fixed tissues were processed, paraffin-embedded, and sectioned at 5 μm thickness and H&E stained at UAB's histology core.

Cell lines, antibodies and reagents—Authentication was carried out at UAB's Heflin Center for genomics by STR profiling. Human cell lines were culture in RPMI-1640 (ATCC® 30–2001™) containing L-glutamine, 10% fetal bovine serum (FBS), and 100U of penicillin-streptomycin except OVCAR3, which were cultured with 20% FBS. Patient ascites derived EOC15 and AF68 cells were culture in 1:1 MCDB 105 and MCDB 131 with 15% FBS. HEK293 cells were maintained in complete DMEM supplemented with L-glutamine, 10% FBS, and penicillin-streptomycin. All cell lines were maintained at 37°C

in a humidified incubator at 5% CO_2, routinely checked for mycoplasma (MycoAlert PLUS mycoplasma detection kit, Lonza, Basel, Switzerland), and experiments conducted within 3–6 passages of testing depending on the cell line. Luc-GFP cell lines were generated using pHIV-Luc-ZsGreen construct. PA1 and SKOV3 cells were transduced followed by cell sorting at the UAB Flow Cytometry Core to generate stable PA1-Luc-GFP and SKOV3-Luc-GFP cells.

METHOD DETAILS

RNA interference and over-expression—Sequences for all constructs and primers are in Tables S1, S2 and S3. Lentiviral particles were generated as previously described (Varadaraj et al., 2015). For stable SMAD1 knockdown, cells were infected with a pool of three individual SMAD1 shRNA lentivirus or non-targeting control (NTC) constructs in complete RPMI media. The media was changed after 24 hr to fresh RPMI supplemented with 10% FBS and 1×PS and left for an additional 48 hr. siRNA-mediated knock-down of SMAD3 and SOX2 was achieved using a pool of two independent siRNA duplexes to SMAD3 or SOX2, respectively and a scrambled siRNA duplex used as a negative control. Transfection was performed using Lipofectamine RNAimax reagent. Briefly, 1×10^5 cells were cultured in 6 well plates in full serum medium for 24 hours. Medium was replaced with 1 mL Opti-MEM, containing 10 nM siRNA duplexes and 7.5 μL Lipofectamine RNAimax. After 15–24 hours, 1 mL 10% serum medium was added to the cells and incubated for 72 hours. The knockdown was confirmed by qRT-PCR (see in Table S1) and/or western blotting. For adenovirus infection, cells were infected with 100 MOI of adenovirus construct expressing ALK2 (Q-D)-HA, ALK3 (Q-D)-HA, generously provided by Gerard C. Blobe and Miyazono K. Transient DNA transfections were carried out in PA1 cells using Lipofectamine LTX dissolved in Opti-MEM medium. For SOX2 overexpression cell lines, indicated cells were infected with EF1A-SOX2 and LV-CMV-SOX2 lentivirus and their respective controls (see Table S1) independently in complete RPMI media with polybrene for 24 hr per instructions. The media was then changed to fresh growth media and incubated for 48 hr, followed by puromycin selection.

Anchorage-independence suspension anoikis assays—For Live/Dead analysis under anchorage independence, 1,000 cells were seeded in 96-well hydrogel-coated ultra-low attachment (ULA) plates (Corning #4515) for times indicated. Growth factor treatment was done under low serum 2.5% FBS condition (Cells were plated in 10% FBS to allow spheroid formation before beginning treatment). Cells were then stained with 2 μM Calcein-AM and 4 μM Ethidium-homodimer for 30 min before imaging. z-stacked images were obtained using the Zeiss LSM700 Confocal microscope (Microscopy and Flow Cytometry Core, University of South Carolina) and NIKON A1 Confocal microscope (UAB High Resolution Imaging Facility). Fluorescent quantification was performed using ImageJ Fiji software to calculate the Corrected Total Cell Fluorescent (CTCF) = Integrated Density – (Area of selected cell × Mean fluorescence of background readings) per spheroid.

Lysate and RNA preparation: 100,000–300,000 cells were seeded in a poly-HEMA coated 6-well plate for indicated times in full serum unless indicated otherwise. Cells were collected

by centrifugation and lysed with trizol for RNA extraction or direct 2x lysis buffer for protein lysates.

3D spheroid invasion—Spheroid invasion through Matrigel was performed as previously described (Vinci et al., 2015) using 1,000 cells that were allowed to form spheroids in ULA wells for 72 hrs. Specifically, Matrigel was mixed with BMP2 and BMP9 to ensure a final concentration of 10nM and added gently to the spheroids in the well, then incubated at 37°C for 1 hr to allow Matrigel solution to solidify. Additional growth media with BMP was added to each well as the top layer. Invasion was then monitored for up to 120 hr. Quantification of the amount of spread/invasion was done using ImageJ software.

Sulforhodamine B (SRB) growth assay—Growth of cells was monitored by seeding 1,000 cells per well in a 96 well plate, followed by treatment with 10 nM BMP2/9 for indicated times. At endpoint, medium was shaken out from plates, followed by addition of cold 10% trichloroacetic acid in each well, and incubation at 4°C for 10 minutes. Five sequential wash steps were performed by complete immersion in water and shake out of the water from the plate. Next, 0.4% sulforhodamine B (SRB) in 1% acetic acid was added to each well and incubated at room temperature for 10 minutes. Five washed were done by complete immersion in 1% acetic acid followed by complete removal of the remaining wash. Plates were air dried overnight. Finally, 200 μL of 20mM Tris pH 10 (unbuffered) was added to each well and plate rocked on a rotary shaker for 1–2 hrs and absorbance measured at 570 nm with a plate reader (Vichai and Kirtikara, 2006).

Immunohistochemistry (IHC) and TUNEL assay—IHC was performed using the BioCare Mach4 Universal Detection Kit. Specifically, anti-SOX2 was diluted in Da Vinci Green Diluent and incubated overnight at 4°C in a humidified chamber. HRP was detected with 3,3′-diaminobenzidine (DAB) substrate for 4 minutes. TUNEL staining was performed according to the manufacturer's instruction. Slides were examined and images captured with EVOS M7000 microscope. Cell profiler (Stirling et al., 2021) and Image J Fiji software were used for image quantification.

Microarray and RNA sequencing—Total cellular RNA was extracted using Trizol reagent according to the manufacturer's protocol. RNA quality was determined using an Agilent 2100 Bioanalyzer and an RNA 6000 Nano kit (Agilent, Cat. No. 5067–1511) with RNA integrity numbers (RIN) ranging from 9.8 to 10. Microarray analysis were performed on the GeneChip™ Human Gene 2.0 ST ArrayS (Thermo Fisher Scientific, Cat. No. 902112) by the functional genomic core at University of South Carolina. Data were imported into the Affymetrix GeneChip Expression Console 1.4.1.46 and processed at the gene-level using the Robust Multichip Analysis (RMA) algorithm to generate CHP files.

Experimental-group specific transcriptional responses were determined using unpaired one-way between-subject analysis of variance (ANOVA). Differentially expressed genes with p-values smaller than 0.05 and fold change higher than 2.0 and lower than −2.0 were used for further bioinformatics analysis.

For RNA sequencing: library preparation was performed on purified, extracted RNA using a KAPA mRNA HyperPrep Kit (Kapa, Biosystems, Wilmington, MA) according to the manufacturer's protocol. High throughput sequencing with 75-bp single-end reads was performed on an Illumina NextSeq 550 using an Illumina NextSeq 500/550 High Output Kit. Reads were aligned to the human transcriptome GENCODE v35 (GRCh38.p13) using STAR and counted using Salmon (Dobin et al., 2013; Patro et al., 2017). Normalization and differential expression analysis were performed using the R package DESeq2 (Love et al., 2014). Genes where there were fewer than three samples with normalized counts less than or equal to five were filtered out of the final data set. Benjamini-Hochberg-adjusted p-value of $p < 0.05$ and log2 fold change of 1 were the thresholds used to identify differentially expressed genes between treatment conditions.

Primary EOC and patient ascitic fluid ELISAs—For cells from patient ascites with an initial diagnosis of high-grade serous adenocarcinoma were collected after informed consent at the Pennsylvania State University College of Medicine (Hershey, PA) or the University of Alabama Birmingham, with approval for the study granted from the Penn State College of Medicine and UAB Institutional Review Boards (IRB). Epithelial cancer cells were isolated from ascites, as previously described (Kim et al., 2020) and used to derive EOC15 and AF68 cells respectively. AF68 was subsequently determined to favor an upper GI primary tumor with a less likely gynecological origin. For the ELISA study, ascites from patients with a confirmed diagnosis of primary OC were analyzed. Ascitic fluid was collected and banked after informed consent at Duke University Medical Center, with approval for the study from Duke University's IRB. Single plex ELISAs were carried out for TGF-β1 and TGF-β2 using Aushon Biosystems Custom Circa Chemiluminescent Array kit while BMP9 was detected as described previously (Liu et al., 2018).

Luciferase assay—HEK293 cells were transfected with the pGL3-SOX2 promoter-luciferase reporter plasmid construct and SV40-renilla for 24h. Treatment with BMP2 or BMP9 or TGF-β or Activin A was carried out for 24 hr in serum-free media at either 10nM or 400pM respectively.

According to the manufacturer's instruction, cells were collected and lysed in 1 × passive lysis buffer. To measure luciferase activity, 20 μL of lysate was added to 25 μL of dual Luciferase Assay Reagent, and luminescence was quantitated using a luminometer (Biotek).

Chromatin immunoprecipitation (ChIP) assay—ChIP was carried out using a modified version of a previously described protocol (Medeiros et al., 2009). Cells were grown to 80% confluency in 150mm culture dishes. Cells were fixed at room temperature in 1% Paraformaldehyde solution (dilute 8% PFA in serum free media to get 1%) and rocked for 10 minutes. 10x Glycine was added to the plate and allowed to sit for 5 minutes at room temperature. Cells were scraped down and cell suspension were transferred to a cold centrifuge tube for centrifugation at 720 RCF at 4°C for 10 minutes. Cells were rinsed with 1X Phosphate buffer saline and centrifugation repeated. Cell pellet was next resuspended in lysis buffers described in (Medeiros et al., 2009) to obtain nuclei pellet. This was followed by chromatin sonication, using QSonica sonicator (model CL-188) for four cycles (30% amplitude for 15secs ON and 30secs OFF) to obtain DNA fragments with a length from 150

to 300 bp. 1/10th of the supernatant was stored as input control. ChIP was performed using Protein A magnetic beads (Dynabeads, Invitrogen #10001D) to couple 3.5 μg ChIP-grade antibodies for SMAD1, SMAD3, H3K27me3, H3K4me3, or rabbit IgG antibody overnight at 4°C. DNA was purified using the PureLink Quick PCR Purification kit (Thermo Fisher Cat #: K310001) and enrichment of DNA fragments analyzed via relative quantitative RT-PCR (qPCR) using ChIP primers (see Table S2) to specific locations. Negative and positive control regions were included in all analysis.

***Methylation-specific* quantitative RT *PCR*—**Genomic DNA was extracted, and bisulfite conversion was performed on 500ng of gDNA using the MethylAmp DNA modification kit according to manufacturer's instructions. Relative quantitative RT-PCR (qPCR) was performed with methylation-specific and unmethylation-specific primers (see Table S3).

QUANTIFICATION AND STATISTICAL ANALYSIS

Xenograft data were analyzed using parametric statistics as described in the legends. Survival curves were analyzed with log-rank statistics. *In vitro* experiments were analyzed using parametric statistics (ANOVA global test with Dunnett's/Sidak multiple comparison test as post-hoc tests as applicable and described in legend) and presented as the mean ± SEM. All real time PCR's are relative semi quantitative RT-PCR's (hereby referred to as qRT-PCR) and are a combined quantitation of a minimum of 3 independent biological trials assayed in triplicate with biological replicates represented as individual scatter dots in the graphs or as indicated in legends. In all cases, statistical significance was set at a threshold of $p < 0.05$. All statistical analyses were conducted with GraphPad Prism Software Ver. 9.0 and specific statistical test information described in figure legends.

Supplementary Material

Refer to Web version on PubMed Central for supplementary material.

ACKNOWLEDGMENTS

We thank Pratik Patel and Drs. A. Varadaraj, L. Vaughn, M. Gatza, E. Listik, S. Murphy, Z. Huang, S. Pradhan, and S. Varambally for discussions, technical assistance, and gifts of cell lines and EZH2 inhibitor. Graphical abstract was made with Biorender.com. Imaging was supported by the UAB HRIF. Funding provided by NIH R01CA230628 to K.M. and N.H., and Ovarian Cancer Research Alliance's Liz Tilberisgrant to K.M.

REFERENCES

Acanda de la Rocha AM, López-Bertoni H, Guruceaga E, González-Huarriz M, Martínez-Vélez N, Xipell E, Fueyo J, Gomez-Manzano C, and Alonso MM (2016). Analysis of SOX2-regulated transcriptome in glioma stem cells. PLoS One 11, e0163155. 10.1371/journal.pone.0163155. [PubMed: 27669421]

Ahmed N, and Stenvers KL (2013). Getting to know ovarian cancer ascites: opportunities for targeted therapy-based translational research. Front. Oncol 3, 256. 10.3389/fonc.2013.00256. [PubMed: 24093089]

Akiyama T, Shida T, Yoshitomi H, Takano S, Kagawa S, Shimizu H, Ohtsuka M, Kato A, Furukawa K, and Miyazaki M (2016). Expression of sex determining region Y-box 2 and pancreatic

and duodenal homeobox 1 in pancreatic neuroendocrine tumors. Pancreas 45, 522–527. 10.1097/mpa.0000000000000504. [PubMed: 26491904]

Alonso MM, Diez-Valle R, Manterola L, Rubio A, Liu D, Cortes-Santiago N, Urquiza L, Jauregi P, de Munain AL, Sampron N, et al. (2011). Genetic and epigenetic modifications of Sox2 contribute to the invasive phenotype of malignant gliomas. PLoS One 6, e26740. 10.1371/journal.pone.0026740. [PubMed: 22069467]

Bååth M, Westbom-Fremer S, Martin de La Fuente L, Ebbesson A, Davis J, Malander S, Måsbäck A, Kannisto P, and Hedenfalk I (2020). SOX2 is a promising predictor of relapse and death in advanced stage high-grade serous ovarian cancer patients with residual disease after debulking surgery. Mol. Cell Oncol 7, 1805094. 10.1080/23723556.2020.1805094. [PubMed: 33235906]

Bani-Yaghoub M, Tremblay RG, Lei JX, Zhang D, Zurakowski B, Sandhu JK, Smith B, Ribecco-Lutkiewicz M, Kennedy J, Walker PR, and Sikorska M (2006). Role of Sox2 in the development of the mouse neocortex. Dev. Biol 295, 52–66. 10.1016/j.ydbio.2006.03.007. [PubMed: 16631155]

Bareiss PM, Paczulla A, Wang H, Schairer R, Wiehr S, Kohlhofer U, Rothfuss OC, Fischer A, Perner S, Staebler A, et al. (2013). SOX2 expression associates with stem cell state in human ovarian carcinoma. Cancer Res. 73, 5544–5555. 10.1158/0008-5472.can-12-4177. [PubMed: 23867475]

Belotte J, Fletcher NM, Alexis M, Morris RT, Munkarah AR, Diamond MP, and Saed GM (2015). Sox2 gene amplification significantly impacts overall survival in serous epithelial ovarian cancer. Reprod. Sci 22, 38–46. 10.1177/1933719114542021. [PubMed: 25038052]

Boergermann JH, Kopf J, Yu PB, and Knaus P (2010). Dorsomorphin and LDN-193189 inhibit BMP-mediated Smad, p38 and Akt signalling in C2C12 cells. Int. J. Biochem. Cell Biol 42, 1802–1807. 10.1016/j.biocel.2010.07.018. [PubMed: 20691279]

Cai Q, Yan L, and Xu Y (2015). Anoikis resistance is a critical feature of highly aggressive ovarian cancer cells. Oncogene 34, 3315–3324. 10.1038/onc.2014.264. [PubMed: 25132267]

Canali S, Core AB, Zumbrennen-Bullough KB, Merkulova M, Wang CY, Schneyer AL, Pietrangelo A, and Babitt JL (2016). Activin B induces noncanonical SMAD1/5/8 signaling via BMP type I receptors in hepatocytes: evidence for a role in hepcidin induction by inflammation in male mice. Endocrinology 157, 1146–1162. 10.1210/en.2015-1747. [PubMed: 26735394]

Candia AF, Watabe T, Hawley SH, Onichtchouk D, Zhang Y, Derynck R, Niehrs C, and Cho KW (1997). Cellular interpretation of multiple TGF-beta signals: intracellular antagonism between activin/BVg1 and BMP-2/4 signaling mediated by Smads. Development 124, 4467–4480. 10.1242/dev.124.22.4467. [PubMed: 9409665]

Cao Z, Livas T, and Kyprianou N (2016). Anoikis and EMT: lethal “liaisons” during cancer progression. Crit. Rev. Oncog 21, 155–168. 10.1615/critrevoncog.2016016955. [PubMed: 27915969]

Card DAG, Hebbar PB, Li L, Trotter KW, Komatsu Y, Mishina Y, and Archer TK (2008). Oct4/Sox2-regulated miR-302 targets cyclin D1 in human embryonic stem cells. Mol. Cell Biol 28, 6426–6438. 10.1128/MCB.00359-08. [PubMed: 18710938]

David CJ, and Massagué J (2018). Contextual determinants of TGFβ action in development, immunity and cancer. Nat. Rev. Mol. Cell Biol 19, 419–435. 10.1038/s41580-018-0007-0. [PubMed: 29643418]

David L, Mallet C, Mazerbourg S, Feige JJ, and Bailly S (2007). Identification of BMP9 and BMP10 as functional activators of the orphan activin receptor-like kinase 1 (ALK1) in endothelial cells. Blood 109, 1953–1961. 10.1182/blood-2006-07-034124. [PubMed: 17068149]

Dobin A, Davis CA, Schlesinger F, Drenkow J, Zaleski C, Jha S, Batut P, Chaisson M, and Gingeras TR (2013). STAR: ultrafast universal RNA-seq aligner. Bioinformatics 29, 15–21. 10.1093/bioinformatics/bts635. [PubMed: 23104886]

Doré JJ, Edens M, Garamszegi N, and Leof EB (1998). Heteromeric and homomeric transforming growth factor-beta receptors show distinct signaling and endocytic responses in epithelial cells. J. Biol. Chem 273, 31770–31777. 10.1074/jbc.273.48.31770. [PubMed: 9822641]

Ehlers MR, and Todd RM (2017). Genesis and maintenance of attentional biases: the role of the locus coeruleus-noradrenaline system. Neural Plast. 2017, 6817349. 10.1155/2017/6817349. [PubMed: 28808590]

Ehrlich M, Gutman O, Knaus P, and Henis YI (2012). Oligomeric interactions of TGF-beta and BMP receptors. FEBS Lett. 586, 1885–1896. 10.1016/j.febslet.2012.01.040. [PubMed: 22293501]

Engers DW, Frist AY, Lindsley CW, Hong CC, and Hopkins CR (2013). Synthesis and structure-activity relationships of a novel and selective bone morphogenetic protein receptor (BMP) inhibitor derived from the pyrazolo[1.5-a]pyrimidine scaffold of dorsomorphin: the discovery of ML347 as an ALK2 versus ALK3 selective MLPCN probe. Bioorg. Med. Chem. Lett 23, 3248–3252. 10.1016/j.bmcl.2013.03.113. [PubMed: 23639540]

Frisch SM, and Francis H (1994). Disruption of epithelial cell-matrix interactions induces apoptosis. J. Cell Biol 124, 619–626. 10.1083/jcb.124.4.619. [PubMed: 8106557]

Frisch SM, Schaller M, and Cieply B (2013). Mechanisms that link the oncogenic epithelial-mesenchymal transition to suppression of anoikis. J. Cell Sci 126, 21–29. 10.1242/jcs.120907. [PubMed: 23516327]

Hao J, Daleo MA, Murphy CK, Yu PB, Ho JN, Hu J, Peterson RT, Hatzopoulos AK, and Hong CC (2008). Dorsomorphin, a selective small molecule inhibitor of BMP signaling, promotes cardiomyogenesis in embryonic stem cells. PLoS One 3, e2904. 10.1371/journal.pone.0002904. [PubMed: 18682835]

Heldin C-H, and Moustakas A (2016). Signaling receptors for TGF-β family members. Cold Spring Harb. Perspect. Biol 8, a022053. 10.1101/cshperspect.a022053. [PubMed: 27481709]

Hellner K, Miranda F, Fotso Chedom D, Herrero-Gonzalez S, Hayden DM, Tearle R, Artibani M, Karaminejadranjbar M, Williams R, Gaitskell K, et al. (2016). Premalignant SOX2 overexpression in the fallopian tubes of ovarian cancer patients: discovery and validation studies. EBioMedicine 10, 137–149. 10.1016/j.ebiom.2016.06.048. [PubMed: 27492892]

Hill CS (2016). Transcriptional control by the SMADs. Cold Spring Harb. Perspect. Biol 8, a022079. 10.1101/cshperspect.a022079. [PubMed: 27449814]

Holtzhausen A, Golzio C, How T, Lee YH, Schiemann WP, Katsanis N, and Blobe GC (2014). Novel bone morphogenetic protein signaling through Smad2 and Smad3 to regulate cancer progression and development. FASEB J. 28, 1248–1267. 10.1096/fj.13-239178. [PubMed: 24308972]

Huang H, Li YJ, Lan CY, Huang QD, Feng YL, Huang YW, and Liu JH (2013). Clinical significance of ascites in epithelial ovarian cancer. Neo-plasma 60, 546–552. 10.4149/neo_2013_071.

Ikushima H, Todo T, Ino Y, Takahashi M, Miyazawa K, and Miyazono K (2009). Autocrine TGF-beta signaling maintains tumorigenicity of glioma-initiating cells through Sry-related HMG-box factors. Cell Stem Cell 5, 666. 10.1016/j.stem.2009.11.011.

Imamura T, Takase M, Nishihara A, Oeda E, Hanai J-I, Kawabata M, and Miyazono K (1997). Smad6 inhibits signalling by the TGF-β superfamily. Nature 389, 622–626. 10.1038/39355. [PubMed: 9335505]

Inman GJ, Nicolás FJ, Callahan JF, Harling JD, Gaster LM, Reith AD, Laping NJ, and Hill CS (2002). SB-431542 is a potent and specific inhibitor of transforming growth factor-beta superfamily type I activin receptor-like kinase (ALK) receptors ALK4, ALK5, and ALK7. Mol. Pharmacol 62, 65–74. 10.1124/mol.62.1.65. [PubMed: 12065756]

Ji J, Ding K, Luo T, Zhang X, Chen A, Zhang D, Li G, Thorsen F, Huang B, Li X, and Wang J (2021). TRIM22 activates NF-κB signaling in glioblastoma by accelerating the degradation of IκBα. Cell Death Differ. 28, 367–381. 10.1038/s41418-020-00606-w. [PubMed: 32814880]

Kelberman D, Rizzoti K, Avilion A, Bitner-Glindzicz M, Cianfarani S, Collins J, Chong WK, Kirk JMW, Achermann JC, Ross R, et al. (2006). Mutations within Sox2/SOX2 are associated with abnormalities in the hypothalamo-pituitary-gonadal axis in mice and humans. J. Clin. Invest 116, 2442–2455. 10.1172/JCI28658. [PubMed: 16932809]

Kim YS, Gupta Vallur P, Jones VM, Worley BL, Shimko S, Shin DH, Crawford LC, Chen CW, Aird KM, Abraham T, et al. (2020). Context-dependent activation of SIRT3 is necessary for anchorage-independent survival and metastasis of ovarian cancer cells. Oncogene 39, 1619–1633. 10.1038/s41388-019-1097-7. [PubMed: 31723239]

Lachmann A, Xu H, Krishnan J, Berger SI, Mazloom AR, and Ma'ayan A (2010). ChEA: transcription factor regulation inferred from integrating genome-wide ChIP-X experiments. Bioinformatics 26, 2438–2444. 10.1093/bioinformatics/btq466. [PubMed: 20709693]

Lane D, Matte I, Garde-Granger P, Laplante C, Carignan A, Rancourt C, and Piché A (2015). Inflammation-regulating factors in ascites as predictive biomarkers of drug resistance and progression-free survival in serous epithelial ovarian cancers. BMC Cancer 15, 492. 10.1186/s12885-015-1511-7. [PubMed: 26122176]

Lim LS, Loh YH, Zhang W, Li Y, Chen X, Wang Y, Bakre M, Ng HH, and Stanton LW (2007). Zic3 is required for maintenance of pluripotency in embryonic stem cells. Mol. Biol. Cell 18, 1348–1358. 10.1091/mbc.e06-07-0624. [PubMed: 17267691]

Liu IM, Schilling SH, Knouse KA, Choy L, Derynck R, and Wang XF (2009). TGFbeta-stimulated Smad1/5 phosphorylation requires the ALK5 L45 loop and mediates the pro-migratory TGFbeta switch. EMBO J. 28, 88–98. 10.1038/emboj.2008.266. [PubMed: 19096363]

Liu Y, Starr MD, Brady JC, Rushing C, Pang H, Adams B, Alvarez D, Theuer CP, Hurwitz HI, and Nixon AB (2018). Modulation of circulating protein biomarkers in cancer patients receiving bevacizumab and the anti-endoglin antibody, TRC105. Mol. Cancer Ther 17, 2248–2256. 10.1158/1535-7163.mct-17-0916. [PubMed: 29997150]

Love MI, Huber W, and Anders S (2014). Moderated estimation of fold change and dispersion for RNA-seq data with DESeq2. Genome Biol. 15, 550. 10.1186/s13059-014-0550-8. [PubMed: 25516281]

Luo J, Tang M, Huang J, He BC, Gao JL, Chen L, Zuo GW, Zhang W, Luo Q, Shi Q, et al. (2010). TGFβ/BMP type I receptors ALK1 and ALK2 are essential for BMP9-induced osteogenic signaling in mesenchymal stem cells. J. Biol. Chem 285, 29588–29598. 10.1074/jbc.m110.130518. [PubMed: 20628059]

Martin-Malpartida P, Batet M, Kaczmarska Z, Freier R, Gomes T, Aragón E, Zou Y, Wang Q, Xi Q, Ruiz L, et al. (2017). Structural basis for genome wide recognition of 5-bp GC motifs by SMAD transcription factors. Nat. Commun 8, 2070. 10.1038/s41467-017-02054-6. [PubMed: 29234012]

Martinez-Hackert E, Sundan A, and Holien T (2021). Receptor binding competition: a paradigm for regulating TGF-beta family action. Cytokine Growth Factor Rev. 57, 39–54. 10.1016/j.cytogfr.2020.09.003. [PubMed: 33087301]

McCabe MT, Ott HM, Ganji G, Korenchuk S, Thompson C, Van Aller GS, Liu Y, Graves AP, Della Pietra A 3rd, Diaz E, et al. (2012). EZH2 inhibition as a therapeutic strategy for lymphoma with EZH2-activating mutations. Nature 492, 108–112. 10.1038/nature11606. [PubMed: 23051747]

Medeiros RB, Papenfuss KJ, Hoium B, Coley K, Jadrich J, Goh S-K, Elayaperumal A, Herrera JE, Resnik E, and Ni H-T (2009). Novel sequential ChIP and simplified basic ChIP protocols for promoter co-occupancy and target gene identification in human embryonic stem cells. BMC Biotechnol. 9, 59. 10.1186/1472-6750-9-59. [PubMed: 19563662]

Miyazono K, Maeda S, and Imamura T (2005). BMP receptor signaling: transcriptional targets, regulation of signals, and signaling cross-talk. Cytokine Growth Factor Rev. 16, 251–263. 10.1016/j.cytogfr.2005.01.009. [PubMed: 15871923]

Monavarian M, Elhaw AT, Tang PW, Javed Z, Shonibare Z, Scalise CB, Arend R, Jolly MK, Sewell- Loftin MK, Hempel N, and Mythreye K (2022). Emerging perspectives on growth factor metabolic relationships in the ovarian cancer ascites environment. Semin. Cancer Biol 10.1016/j.semcancer.2022.03.004.

Naber HPH, Wiercinska E, Ten Dijke P, and Van Laar T (2011). Spheroid assay to measure TGF-β-induced invasion. J. Vis. Exp, 3337. 10.3791/3337. [PubMed: 22126971]

Neckmann U, Wolowczyk C, Hall M, Almaas E, Ren J, Zhao S, Johannessen B, Skotheim RI, Bjørkøy G, Ten Dijke P, and Holien T (2019). GREM1 is associated with metastasis and predicts poor prognosis in ER-negative breast cancer patients. Cell Commun. Signal 17, 140. 10.1186/s12964-019-0467-7. [PubMed: 31694641]

Ochieng JK, Schilders K, Kool H, Boerema-De Munck A, Buscop-Van Kempen M, Gontan C, Smits R, Grosveld FG, Wijnen RMH, Tibboel D, and Rottier RJ (2014). Sox2 regulates the emergence of lung basal cells by directly activating the transcription of Trp63. Am. J. Respir. Cell Mol. Biol 51, 311–322. 10.1165/rcmb.2013-0419oc. [PubMed: 24669837]

Olsen OE, Wader KF, Misund K, Våtsveen TK, Rø TB, Mylin AK, Turesson I, Størdal BF, Moen SH, Standal T, et al. (2014). Bone morphogenetic protein-9 suppresses growth of myeloma cells by signaling through ALK2 but is inhibited by endoglin. Blood Cancer J. 4, e196. 10.1038/bcj.2014.16. [PubMed: 24658374]

Patro R, Duggal G, Love MI, Irizarry RA, and Kingsford C (2017). Salmon provides fast and bias-aware quantification of transcript expression. Nat. Methods 14, 417–419. 10.1038/nmeth.4197. [PubMed: 28263959]

Peng J, Yoshioka Y, Mandai M, Matsumura N, Baba T, Yamaguchi K, Hamanishi J, Kharma B, Murakami R, Abiko K, et al. (2016). The BMP signaling pathway leads to enhanced proliferation in serous ovarian cancer-A potential therapeutic target. Mol. Carcinog 55, 335–345. 10.1002/mc.22283. [PubMed: 25663289]

Pham DL, Scheble V, Bareiss P, Fischer A, BeschorneR C, Adam A, Bachmann C, Neubauer H, Boesmueller H, Kanz L, et al. (2013). SOX2 expression and prognostic significance in ovarian carcinoma. Int. J. Gynecol. Pathol 32, 358–367. 10.1097/pgp.0b013e31826a642b. [PubMed: 23722508]

Ramachandran A, Vizán P, Das D, Chakravarty P, Vogt J, Rogers KW, Müller P, Hinck AP, Sapkota GP, and Hill CS (2018). TGF-β uses a novel mode of receptor activation to phosphorylate SMAD1/5 and induce epithelialto-mesenchymal transition. Elife 7, e31756. 10.7554/elife.31756. [PubMed: 29376829]

Ren W, Sun X, Wang K, Feng H, Liu Y, Fei C, Wan S, Wang W, Luo J, Shi Q, et al. (2014). BMP9 inhibits the bone metastasis of breast cancer cells by downregulating CCN2 (connective tissue growth factor, CTGF) expression. Mol. Biol. Rep 41, 1373–1383. 10.1007/s11033-013-2982-8. [PubMed: 24413988]

Ross S, and Hill CS (2008). How the Smads regulate transcription. Int. J. Biochem. Cell Biol 40, 383–408. 10.1016/j.biocel.2007.09.006. [PubMed: 18061509]

Scharpfenecker M, Van Dinther M, Liu Z, Van Bezooijen RL, Zhao Q, Pukac L, Löwik CWGM, and Ten Dijke P (2007). BMP-9 signals via ALK1 and inhibits bFGF-induced endothelial cell proliferation and VEGF-stimulated angiogenesis. J. Cell Sci 120, 964–972. 10.1242/jcs.002949. [PubMed: 17311849]

Seki Y (2018). PRDM14 is a unique epigenetic regulator stabilizing transcriptional networks for pluripotency. Front. Cell Dev. Biol 6, 12. 10.3389/fcell.2018.00012. [PubMed: 29487849]

Sholl LM, Barletta JA, Yeap BY, Chirieac LR, and Hornick JL (2010). Sox2 protein expression is an independent poor prognostic indicator in stage I lung adenocarcinoma. Am. J. Surg. Pathol 34, 1193–1198. 10.1097/pas.0b013e3181e5e024. [PubMed: 20631605]

Si J, Ma Y, Bi JW, Xiong Y, Lv C, Li S, Wu N, and Yang Y (2019). Shisa3 brakes resistance to EGFR-TKIs in lung adenocarcinoma by suppressing cancer stem cell properties. J. Exp. Clin. Cancer Res 38, 481. 10.1186/s13046-019-1486-3. [PubMed: 31801598]

Sinclair AH, Berta P, Palmer MS, Hawkins JR, Griffiths BL, Smith MJ, Foster JW, Frischauf AM, Lovell-Badge R, and Goodfellow PN (1990). A gene from the human sex-determining region encodes a protein with homology to a conserved DNA-binding motif. Nature 346, 240–244. 10.1038/346240a0. [PubMed: 1695712]

Singh A, and Morris RJ (2010). The Yin and Yang of bone morphogenetic proteins in cancer. Cytokine Growth Factor Rev. 21, 299–313. 10.1016/j.cytogfr.2010.06.003. [PubMed: 20688557]

Soikkeli J, Podlasz P, Yin M, Nummela P, Jahkola T, Virolainen S, Krogerus L, Heikkilä P, Von Smitten K, Saksela O, and Hölttä E (2010). Metastatic outgrowth encompasses COL-I, FN1, and POSTN up-regulation and assembly to fibrillar networks regulating cell adhesion, migration, and growth. Am. J. Pathol 177, 387–403. 10.2353/ajpath.2010.090748. [PubMed: 20489157]

Soufi A, Donahue G, and Zaret KS (2012). Facilitators and impediments of the pluripotency reprogramming factors' initial engagement with the genome. Cell 151, 994–1004. 10.1016/j.cell.2012.09.045. [PubMed: 23159369]

Stirling DR, Swain-Bowden MJ, Lucas AM, Carpenter AE, Cimini BA, and Goodman A (2021). CellProfiler 4: improvements in speed, utility and usability. BMC Bioinf. 22, 433. 10.1186/s12859-021-04344-9.

Sun C, Sun L, Li Y, Kang X, Zhang S, and Liu Y (2013). Sox2 expression predicts poor survival of hepatocellular carcinoma patients and it promotes liver cancer cell invasion by activating Slug. Med. Oncol 30, 503. 10.1007/s12032-013-0503-1. [PubMed: 23430442]

Tao JJ, Cangemi NA, Makker V, Cadoo KA, Liu JF, Rasco DW, Navarro WH, Haqq CM, and Hyman DM (2019). First-in-Human phase I study of the activin A inhibitor, STM 434, in patients with

granulosa cell ovarian cancer and other advanced solid tumors. Clin. Cancer Res 25, 5458–5465. 10.1158/1078-0432.ccr-19-1065. [PubMed: 31068369]

Tillet E, and Bailly S (2014). Emerging roles of BMP9 and BMP10 in hereditary hemorrhagic telangiectasia. Front. Genet 5, 456. 10.3389/fgene.2014.00456. [PubMed: 25620979]

Torchiaro E, Lorenzato A, Olivero M, Valdembri D, Gagliardi PA, Gai M, Erriquez J, Serini G, and Di Renzo MF (2016). Peritoneal and hematogenous metastases of ovarian cancer cells are both controlled by the p90RSK through a self-reinforcing cell autonomous mechanism. Oncotarget 7, 712–728. 10.18632/oncotarget.6412. [PubMed: 26625210]

Varadaraj A, Patel P, Serrao A, Bandyopadhay T, Lee NY, Jazaeri AA, Huang Z, Murphy SK, and Mythreye K (2015). Epigenetic regulation of GDF2 suppresses anoikis in ovarian and breast epithelia. Neoplasia 17, 826–838. 10.1016/j.neo.2015.11.003. [PubMed: 26678910]

Viallard C, Audiger C, Popovic N, Akla N, Lanthier K, Legault-Navarrete I, Melichar H, Costantino S, Lesage S, and Larrivée B (2020). BMP9 signaling promotes the normalization of tumor blood vessels. Oncogene 39, 2996–3014. 10.1038/s41388-020-1200-0. [PubMed: 32042114]

Vichai V, and Kirtikara K (2006). Sulforhodamine B colorimetric assay for cytotoxicity screening. Nat. Protoc 1, 1112–1116. 10.1038/nprot.2006.179. [PubMed: 17406391]

Vinci M, Box C, and Eccles SA (2015). Three-dimensional (3D) tumor spheroid invasion assay. J. Vis. Exp, e52686. 10.3791/52686. [PubMed: 25993495]

Wakefield LM, and Hill CS (2013). Beyond TGFβ: roles of other TGFβ superfamily members in cancer. Nat. Rev. Cancer 13, 328–341. 10.1038/nrc3500. [PubMed: 23612460]

Wang J, Ding N, Li Y, Cheng H, Wang D, Yang Q, Deng Y, Yang Y, Li Y, Ruan X, et al. (2015). Insulin-like growth factor binding protein 5 (IGFBP5) functions as a tumor suppressor in human melanoma cells. Oncotarget 6, 20636–20649. 10.18632/oncotarget.4114. [PubMed: 26010068]

Wang X, Ji X, Chen J, Yan D, Zhang Z, Wang Q, Xi X, and Feng Y (2014). SOX2 enhances the migration and invasion of ovarian cancer cells via Src kinase. PLoS One 9, e99594. 10.1371/journal.pone.0099594. [PubMed: 24937695]

Wegner M (2010). All purpose Sox: the many roles of Sox proteins in gene expression. Int. J. Biochem. Cell Biol 42, 381–390. 10.1016/j.biocel.2009.07.006. [PubMed: 19631281]

Weina K, and Utikal J (2014). SOX2 and cancer: current research and its implications in the clinic. Clin. Transl. Med 3, 19. 10.1186/2001-1326-3-19. [PubMed: 25114775]

Yamamura S, Matsumura N, Mandai M, Huang Z, Oura T, Baba T, Hamanishi J, Yamaguchi K, Kang HS, Okamoto T, et al. (2012). The activated transforming growth factor-beta signaling pathway in peritoneal metastases is a potential therapeutic target in ovarian cancer. Int. J. Cancer 130, 20–28. 10.1002/ijc.25961. [PubMed: 21503873]

Yang J, Tian X, Yang J, Cui J, Jiang S, Shi R, Liu Y, Liu X, Xu W, Xie W, et al. (2017). 5-Aza-2′-deoxycytidine, a DNA methylation inhibitor, induces cytotoxicity, cell cycle dynamics and alters expression of DNA methyltransferase 1 and 3A in mouse hippocampus-derived neuronal HT22 cells. J. Toxicol. Environ. Health 80, 1222–1229. 10.1080/15287394.2017.1367143.

Ye L, Kynaston H, and Jiang WG (2008). Bone morphogenetic protein-9 induces apoptosis in prostate cancer cells, the role of prostate apoptosis response-4. Mol. Cancer Res 6, 1594–1606. 10.1158/1541-7786.mcr-08-0171. [PubMed: 18922975]

Yeh HW, Hsu EC, Lee SS, Lang YD, Lin YC, Chang CY, Lee SY, Gu DL, Shih JH, Ho CM, et al. (2018). PSPC1 mediates TGF-β1 autocrine signalling and Smad2/3 target switching to promote EMT, stemness and metastasis. Nat. Cell Biol 20, 479–491. 10.1038/s41556-018-0062-y. [PubMed: 29593326]

Yuan G, Zhan Y, Gou X, Chen Y, and Yang G (2018). TGF-β signaling inhibits canonical BMP signaling pathway during palate development. Cell Tissue Res. 371, 283–291. 10.1007/s00441-017-2757-y. [PubMed: 29247325]

Zeisberg M, Hanai J.i., Sugimoto H, Mammoto T, Charytan D, Strutz F, and Kalluri R (2003). BMP-7 counteracts TGF-beta1-induced epithelial-tomesenchymal transition and reverses chronic renal injury. Nat. Med 9, 964–968. 10.1038/nm888. [PubMed: 12808448]

Zhang J, Chang DY, Mercado-Uribe I, and Liu J (2012). Sex-determining region Y-box 2 expression predicts poor prognosis in human ovarian carcinoma. Hum. Pathol 43, 1405–1412. 10.1016/j.humpath.2011.10.016. [PubMed: 22401770]

Zhang Q, Hou X, Evans BJ, Vanblaricom JL, Weroha SJ, and Cliby WA (2018). LY2157299 monohydrate, a TGF-βR1 inhibitor, suppresses tumor growth and ascites development in ovarian cancer. Cancers 10, 260. 10.3390/cancers10080260. [PubMed: 30087253]

Highlights

- SOX2 is a key node for anchorage-independent survival in cancer
- SOX2 levels are differentially balanced by TGF-β/activin and BMPs in cancer
- BMP9 is a robust intraperitoneal metastasis suppressor by lowering SOX2
- SOX2 regulation is contextual and at the transcriptional level

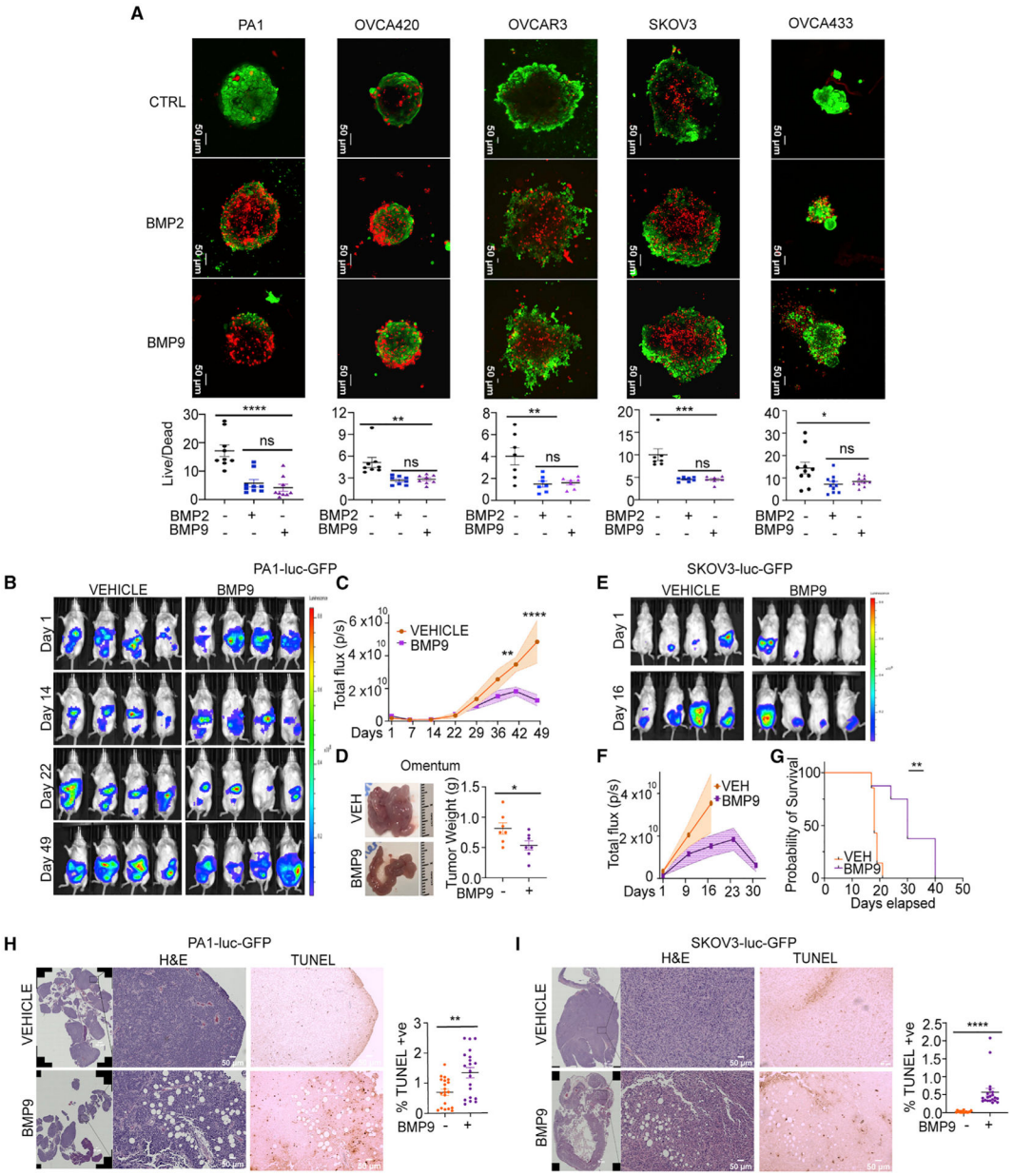

Figure 1. BMPs induce anoikis and suppress OC growth and metastasis *in vivo*

(A) Representative confocal microscopy images of OC cells cultured under anchorage independence for 48 h and subsequently treated with vehicle (VEH) or 10 nM BMP2 or BMP9 for 24 h. Live/dead cell ratios assessed by calcein-AM (green, live cells) and ethidium homodimer dye (red, dead cells). (Scale bar, 50 μm; n = 7–10 spheroids/condition).

(B) Representative tumor luminescence images of NOD-SCID mice injected with PA1-luc-GFP cells with vehicle or rhBMP9 (5 mg/kg) administered i.p. daily (indicated days post-tumor cell injection from 4 mice are shown).

(C) Whole-animal luminescence quantified over time (n = 8 mice for rhBMP9, n = 7 for vehicle).

(D) Representative image of omental tumor burden (left) and quantification of omental tumor weight (right) from mice that received vehicle or rhBMP9 injected with PA1-luc-GFP tumor cells (n = 8 mice for rhBMP9, n = 7 for vehicle).
(E) Representative tumor luminescence images of NOD-SCID mice injected with SKOV3-luc-GFP cells with vehicle or rhBMP9 (5 mg/kg) administered i.p. daily (days 1 and 16 post-tumor cell injection from 4 mice are shown).
(F) Whole-animal luminescence quantified over time (n = 8 for rhBMP9, n = 7 for vehicle).
(G) KM plot of SKOV3-Luc-GFP-injected mice receiving rhBMP9 compared with vehicle.
(H and I) Representative H&E and TUNEL staining of (H) PA1-luc-GFP and (I) SKOV3-luc-GFP tumors. (Scale bar, 50 μm; TUNEL stain quantification is shown for two mice per group per cell line. n = 17–20 random fields/condition) (right: *p < 0.05, **p < 0.01, ***p < 0.001). All data are the mean ± SEM; *p < 0.05, **p < 0.01, ***p < 0.001. Statistical significance determined by (A) ANOVA followed by Dunnett's multiple comparison test and (C–I) unpaired Student's t test (see also Figure S1).

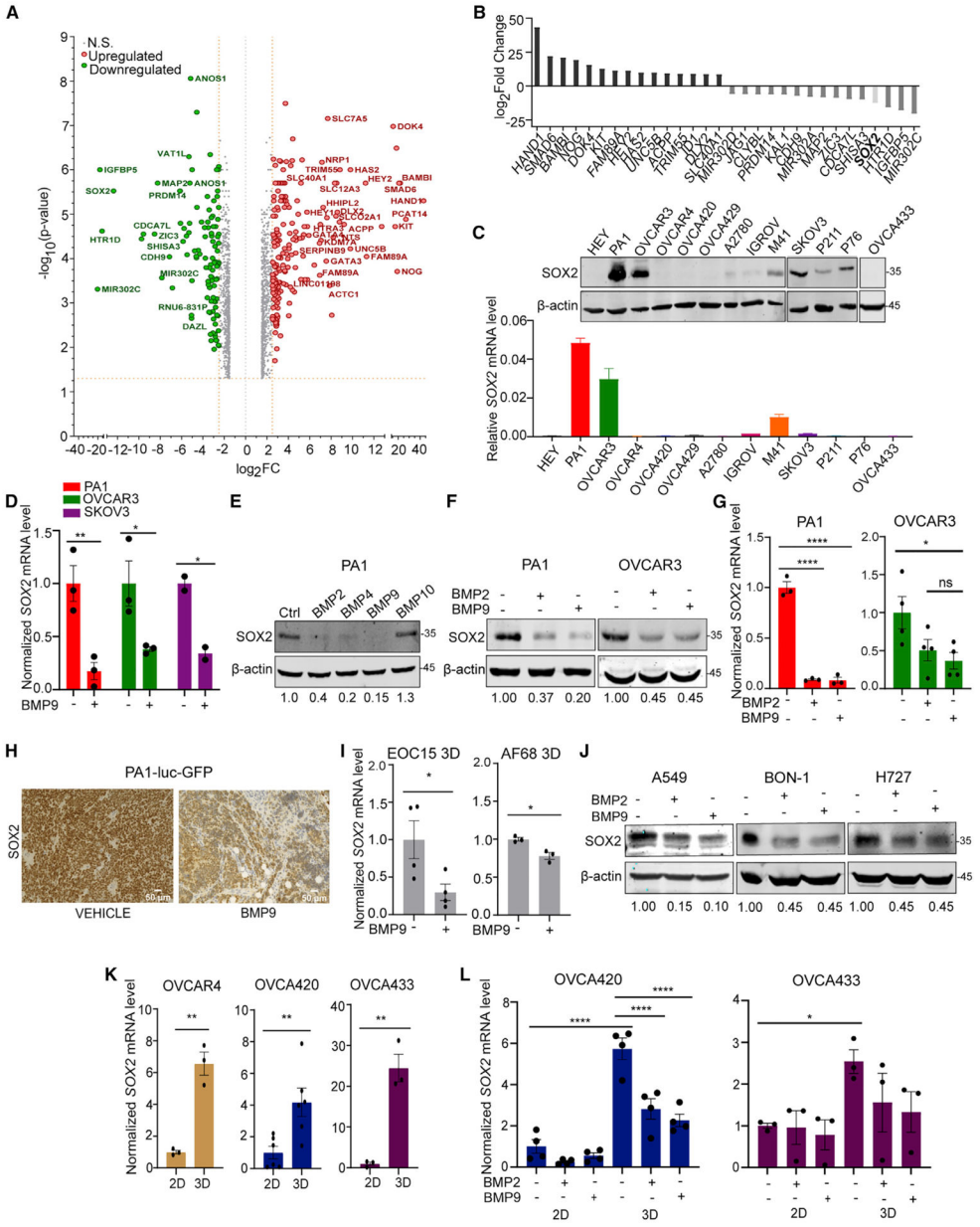

Figure 2. SOX2 is downregulated by BMP2, -4, and -9 in cancer cell lines and xenograft tumors

(A) Volcano plot of changes in gene expression in PA1 cells under anchorage-independence treated with vehicle or rhBMP9 for 24 h (cutoff 1.5 $\log_2$ FC; genes above cutoff of 5 are labeled; n = 3 biological replicates).

(B) List of 15 top upregulated and downregulated genes in response to rhBMP9 from (A).

(C) Western blot (WB; top) and qRT-PCR (bottom) of SOX2 levels in a panel of OC cells (WB: n = 2–5 biological replicates; qPCR: n = 3 technical replicates).

(D) qRT-PCR analysis of *SOX2* mRNA levels in response to 24 h of BMP9 (10 nM) treatment expressed relative to control untreated cells (n = 2–3 biological replicates).

(E) Western blot following treatment with BMP2, -4, and -9 and 10 (10 nM) or control for 24 h in PA1 cells to assess SOX2 protein (n = 2–3 biological replicates). Quantitation of SOX2 relative to actin is presented below.
(F) Western blot of BMP2 and BMP9 treatment and SOX2 protein in PA1 and OVCAR3 cells (n = 2 biological replicates). Quantitation of SOX2 relative to actin is presented below.
(G) qRT-PCR analysis of relative *SOX2* levels after BMP2 and BMP9 treatment normalized to untreated control (n = 3–4 biological replicate).
(H) Representative immunohistochemistry (IHC) of SOX2 in PA1-Luc-GFP tumors from mice receiving vehicle or rhBMP9 from Figure 1B (Scale bar, 50 μm; n = 2 mice/condition).
(I) qRT-PCR analysis of relative *SOX2* transcript levels in patient ascites-derived tumor cells maintained under anchorage independence ± BMP9 for 48 h and normalized to untreated (n = 3–4 biological replicates).
(J) Western blot for SOX2 following treatment with BMP2 or BMP9 for 24 h or control in cell lines of different cancer origin (n = 2, A459 n = 3 biological replicates). Quantitation of SOX2 relative to actin is shown.
(K) qRT-PCR analysis of relative SOX2 increases in anchorage-independent conditions (3D) compared with attached (2D) culture conditions after 72 h (n = 3–6 biological replicates).
(L) qRT-PCR analysis of relative *SOX2* ± BMP2 or BMP9 for 24 h in a 72-h period under anchorage-independent (3D) conditions or attached (2D) conditions (n = 3–4 biological replicates). Data are normalized to untreated attached (2D) conditions in indicated cells for (K) and (L). Data are the mean ± SEM; *p < 0.05, **p < 0.01, ***p < 0.001. Statistical significance determined by ANOVA followed by (D) Sidak's or (G–L) Dunnett's multiple comparison test (see also Figures S2 and S3).

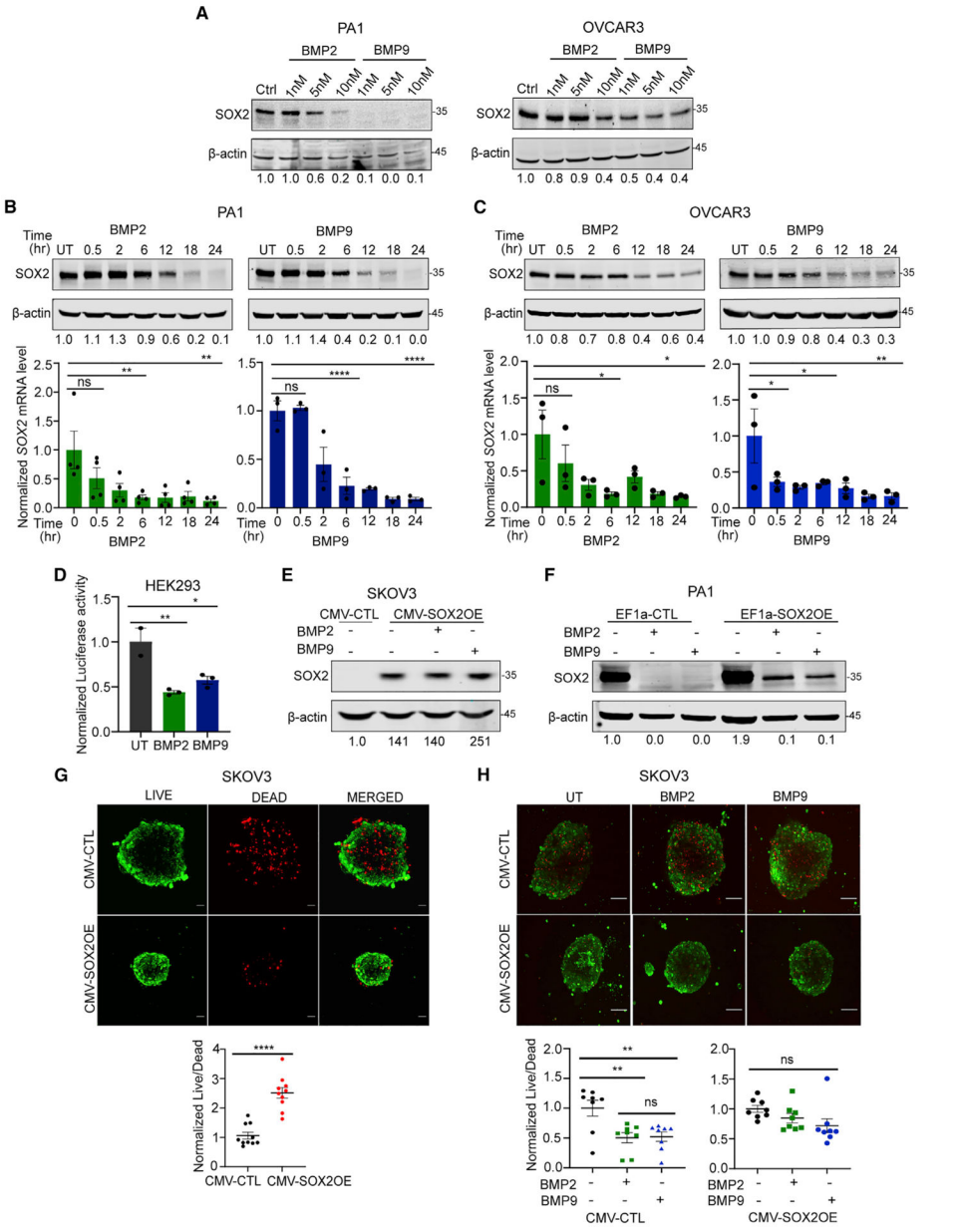

Figure 3. Downregulation of SOX2 is required for anoikis

(A) Western blot of SOX2 protein following BMP treatment with indicated doses for 24 h in PA1 and OVCAR3 cells. Quantitation of SOX2 relative to actin is presented below (n = 3 biological replicates).

(B and C) Time course analysis of SOX2 protein by western blot (top) and relative *SOX2* mRNA by qRT-PCR analysis (bottom) after 10 nM BMP2 and BMP9 treatment, normalized to untreated conditions (time 0 h/UT) in (B) PA1 and (C) OVCAR3 cells (n = 3–4 biological replicates).

(D) pGL3-*SOX2* promoter-reporter luciferase analysis in HEK293 cells following BMP2 and BMP9 treatment for 24 h and normalized to untreated and renilla internal control (n = 2–3 biological replicates).

(E and F) Western blot analysis of effect of BMP2 and BMP9 treatment for 24 h on SOX2 expression in CMV-CTL and CMV-SOX2 cells in (E) SKOV3 (n = 3 biological replicates), and EF1a-CTL and EF1a-SOX2 in (F) PA1 cells (n = 1 biological replicate).

(G) Representative live-dead images from SKOV3 CMV-CTL and CMV-SOX2 cells cultured under anchorage independence for 72 h (top), quantified relative to CMV-CTL control (bottom right, n = 10 spheroids/condition; scale bar, 50 μm. unpaired Student's t test).

(H) Representative images from SKOV3 CMV-CTL and CMV-SOX2 cells ± equimolar BMP2 or BMP9 for 24 h and live/dead ratios quantified relative to untreated controls below (n = 8 spheroids/condition; scale bar, 50 μm). Data are the mean ± SEM; *p < 0.05, **p < 0.01, ***p < 0.001. Statistical significance determined by ANOVA followed by Dunnett's multiple comparison test.

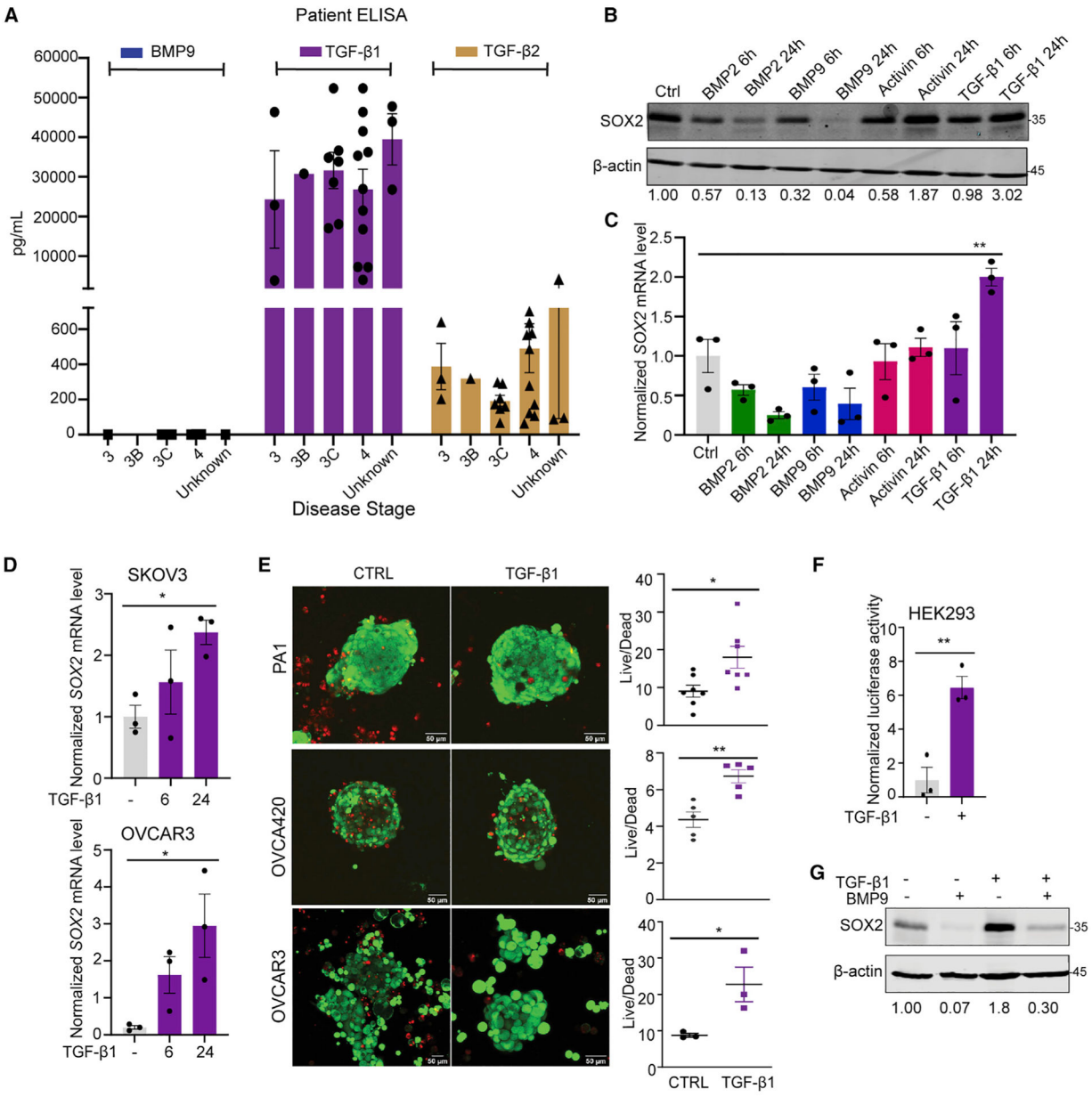

Figure 4. Ovarian cancer (OC) ascites are high in TGF-β ligands, which upregulate SOX2 transcription and suppress anoikis

(A) Concentration of indicated ligands in OC patient-derived ascitic fluid (BMP9, n = 10; TGF-β1, n = 25; TGFβ2, n = 25, where n represents number of patients).

(B) Western blot of SOX2 after treatment with indicated growth factors in PA1 cells. Quantitation of SOX2 relative to actin is presented below (n = 3 biological replicates).

(C) qRT-PCR of *SOX2* after treatment with indicated growth factors for indicated times in PA1 cells (n = 3 biological replicates; ANOVA followed by Dunnett's multiple comparisons test).

(D) Time course analysis of *SOX2* by qRT-PCR after TGF-β1 treatment in indicated cells (n = 3 biological replicates; ANOVA followed by Sidak's multiple comparison test and unpaired Student's t test).

(E) Representative images from live-dead analysis upon TGF-β1 treatment in indicated cells. Quantitation of live/dead ratio in spheroids assessed by calcein-AM (green, live cells) and ethidium homodimer dye (red, dead cells; n = 3–7 spheroids/condition; scale bar, 50 μm).
(F) pGL3-*SOX2* promoter-reporter luciferase analysis upon TGF-β1 treatment for 24 h in HEK293 cells normalized to untreated and renilla internal control (n = 3 biological replicates) (unpaired Student's t test).
(G) Representative western blot of SOX2 after co-treatment of equimolar (1 nM) TGF-β1 and BMP9 for 24 h in PA1 cells (n = 3 biological replicates). Data are the mean ± SEM; *p < 0.05, **p < 0.01, ***p < 0.001 (see also Figure S4).

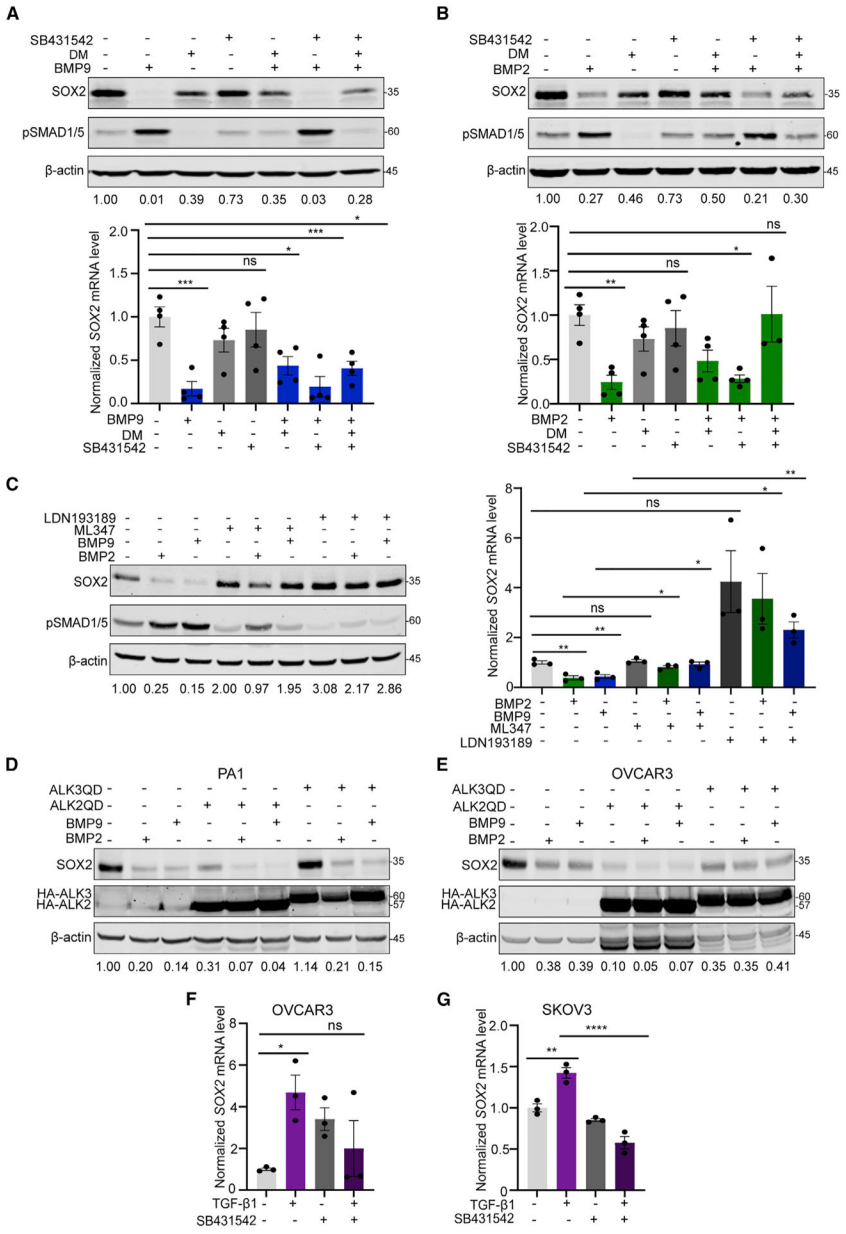

Figure 5. SOX2 is reciprocally regulated by ALK2/ALK3 and ALK5 receptor kinases

(A) Western blot (top) and qRT-PCR (bottom) of SOX2 in PA1 cells pretreated with 5 μM ALK2,3,6 inhibitor dorsomorphin (DM) and 5 μM ALK4/5/7 inhibitor SB431542 for 1 h, followed by treatment with BMP9 for 24 h. Data are normalized to vehicle DMSO controls. Quantitation of SOX2 relative to actin is presented below (WB, n = 3 for DM and n = 2 biological replicates for SB; qPCR: n = 4 biological replicates).

(B) Western blot (top) and qRT-PCR (bottom) analysis of SOX2 in PA1 cells pretreated with 5 μM DM and 5 μM SB431542 for 1 h, followed by treatment with BMP2 for 24 h. Data are normalized to DMSO vehicle controls. Quantitation of SOX2 relative to actin is presented below (n = 4 for DM and n = 2 biological replicates for SB; qPCR: n = 3–4 biological replicates).

(C) Western blot (left) and qRT-PCR (right) analysis of SOX2 in PA1 cells pretreated with 3 μM ALK1,2 inhibitor ML347 and 0.8 μM ALK2,3 LDN193189 for 1 h, followed by treatment with BMP2/9 for 24 h. Data are normalized to vehicle controls presented. Quantitation of SOX2 relative to actin is presented below (WB, n = 2 biological replicates; qRT-PCR, n = 3 biological replicates).

(D and E) Western blot of SOX2 in cells expressing ALK2QD, ALK3QD, or vector control treated for 24 h with equimolar BMP2 and BMP9 in (D) PA1(n = 2 biological replicates) and (E) OVCAR3 (n = 1 biological replicate) cells.

(F and G) qRT-PCR of *SOX2* in indicated cells pretreated with 5 μM SB431542 for 1 h, followed by treatment with 400 pM TGF-β1 for 24 h. Data are normalized to DMSO controls (n = 3 biological replicates). All data are presented as the mean ± SEM; *p < 0.05, **p < 0.01, ***p < 0.001 (A–B) and (F) ANOVA followed by Dunnett's multiple comparison test, (C) Student t test, and (G) ANOVA followed by Sidak's multiple comparison test (see also Figure S5).

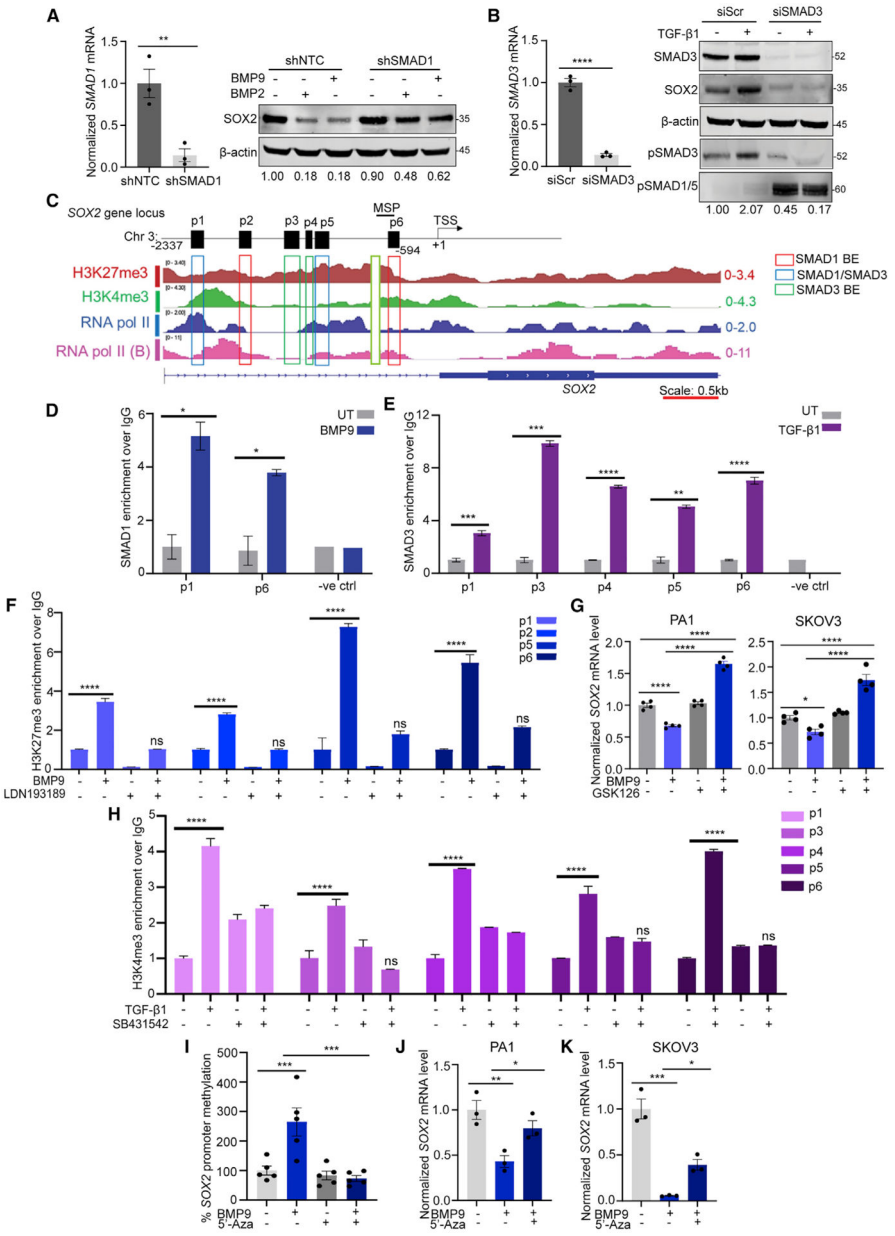

Figure 6. SMAD1 and SMAD3 directly regulate SOX2 expression and occupy *SOX2*'s promoter at distinct and overlapping sites

(A) Representative qRT-PCR of *SMAD1* levels in shSMAD1 cells normalized to shNTC in OVCAR3 cells (left; n = 3 technical replicates). Western blot analysis of SOX2 in OVCAR3 shSMAD1 or non-targeting control (shNTC) cells treated with indicated equimolar BMPs for 24 h (right; n = 3 biological replicates).

(B) qRT-PCR analysis of *SMAD3* in OVCAR3 cells transiently expressing siRNA to SMAD3 (siSMAD3) or scramble control (siScr). Data are normalized to siScr in OVCAR3 cells (left). Western blot analysis of indicated proteins in OVCAR3 siSMAD3 or scramble control (siScr) cells treated with TGF-β1 for 24 h with quantitation of SOX2 relative to actin shown below (right; n = 3 biological replicates).

(C) *In silico* analysis showing primers flanking SMAD1 and SMAD3-binding elements (BE) in chromosomal regions including *SOX2*'s promoter and gene as indicated. TSS, transcription start site; MSP, methylation-specific PCR primer.
(D) Relative qRT-PCR of indicated regions (primer sites) after chromatin immunoprecipitation (ChIP) of SMAD1 with or without 1 h of BMP9 treatment, expressed as the ratio over IgG controls normalized to untreated cells (n = 2 biological replicates).
(E) Representative relative qRT-PCR of indicated regions (primer sites) after ChIP of SMAD3 with or without 1 h of TGF-β1 treatment, expressed as the ratio over IgG controls normalized to untreated cells (n = 3 technical replicates).
(F) Representative qRT-PCR of indicated regions (primer sites) associated with H3K27me3 enrichment with and without 1 h of BMP9 treatment ± LDN193189 as indicated in PA1 cells expressed as the ratio over IgG controls normalized to untreated cells (n = 3 technical replicates).
(G) qRT-PCR analysis of *SOX2* levels in indicated cells pretreated with 5 μM GSK126 for 5 days, followed by treatment with BMP9 for 24 h. Data are normalized to DMSO controls (n = 4 biological replicates).
(H) Representative qRT-PCR of indicated regions (primer sites) after ChIP with H3K4me3 ± 1-h TGF-β1 ± SB431542 as indicated in PA1 cells expressed as the ratio over IgG controls normalized to untreated cells (n = 3 technical replicates).
(I) MS-qPCR using primers proximal to *SOX2*'s TSS (MSP in C) in PA1 cells pretreated with 5 μM 5′-azacytidine (5′-Aza) for 48 h, followed by treatment with BMP9 for 24 h, normalized to DMSO control (n = 5 biological replicates).
(J and K) qRT-PCR analysis of *SOX2* in (J) PA1 and (K) SKOV3 cells treated with 5 μM 5′-Aza and 10 nM BMP9, normalized to DMSO control (n = 3 biological replicates). Data are presented as the mean ± SEM; *$p < 0.05$, **$p < 0.01$, ***$p < 0.001$ (ANOVA followed by Sidak's multiple comparison test) (see also Figures S6 and S7).

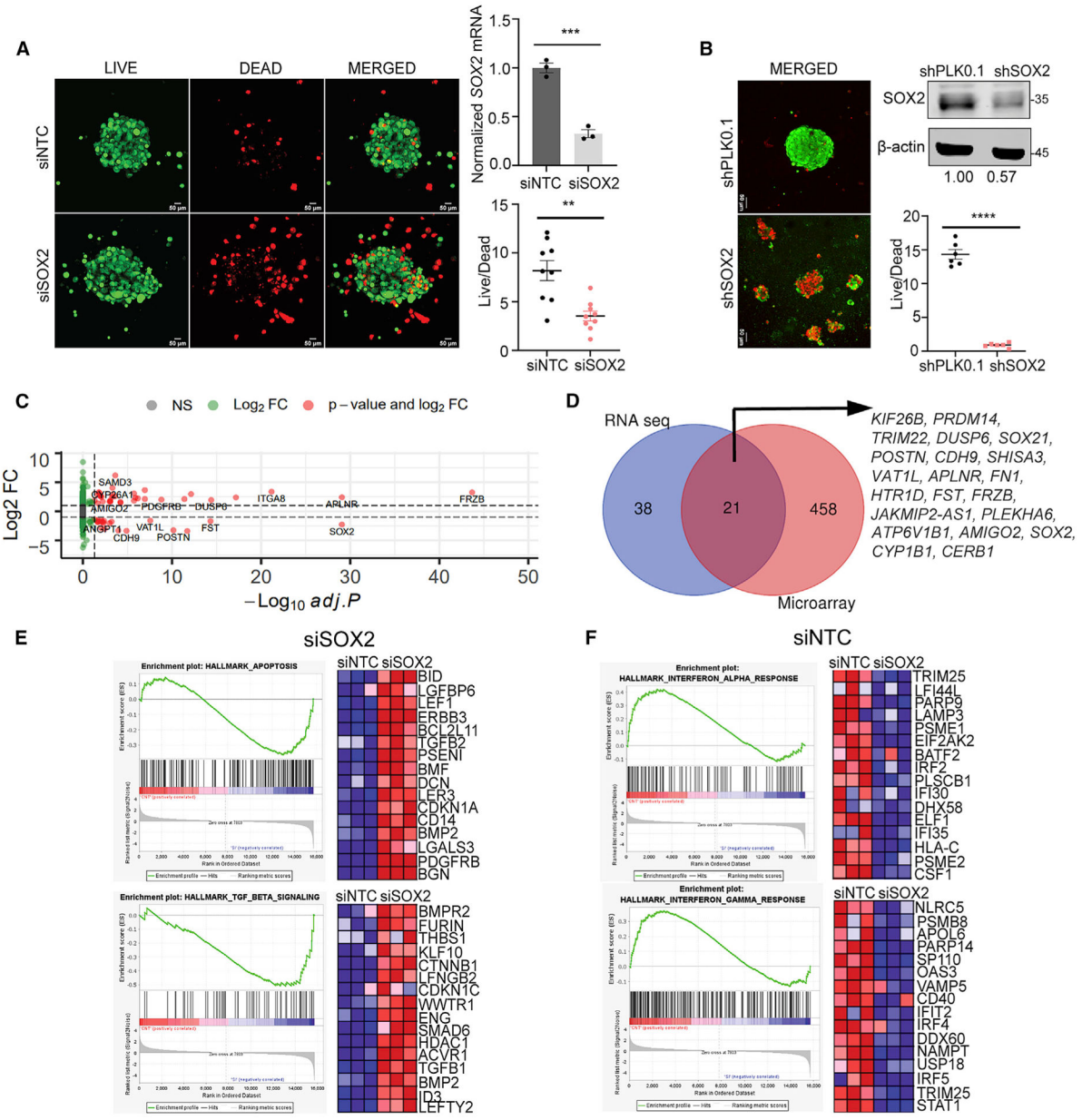

Figure 7. Genome-wide transcriptome changes upon reducing SOX2 and increasing anoikis reveal apoptotic pathways and key transcriptional epigenetic regulators and adhesion molecules

(A) Representative confocal image from siNTC or siSOX2 PA1 cells under anchorage independence for 72 h (left) with quantitation of live/dead ratio (bottom right, n = 9 spheroids/condition. Scale bar, 50 μm). qRT-PCR of SOX2 expression in siSOX2 cells normalized to siNTC cells (top right, n = 3 technical replicates).

(B) Representative images from PA1 shPLKO.1 and shSOX2 cells under anchorage independence for 72 h (left). Western blot of SOX2 in shPLK0.1 and shSOX2 cells (top right), and quantitation of live/dead ratio in spheroid cells (n = 6 spheroids/condition, bottom right. Scale bar, 50 μm). *p < 0.05, **p < 0.01, ***p < 0.001.

(C) Volcano plot of significant DEGs based on adjusted p value of 0.05 between siNTC and siSOX2 in PA1 cells under anchorage independence for 48 h.

(D) Venn diagram of common DEGs between RNA-seq data from (A) and microarray data from BMP9 treatment under anchorage independence in PA1 cells from Figure 2A.
(E and F) Gene set enrichment analysis (GSEA) of pathways differentially altered in (E) siSOX2 and (F) siNTC with corresponding Blue-Pink O'gram of core enrichment genes generated by GSEA (right) (see also Figure S8).

KEY RESOURCES TABLE

REAGENT or RESOURCE	SOURCE	IDENTIFIER
Antibodies		
phospho-SMAD111/5	Cell Signaling Technology	RRID: AB_491015
phospho-SMAD2/3	Cell Signaling Technology	RRID: AB_2631089
SMAD1	Cell Signaling Technology	RRID: AB_10858882
SMAD2/3	Cell Signaling Technology	RRID: AB_10693547
H3K27me3	Cell Signaling Technology	RRID: AB_2616029
H3K4me3	Cell Signaling Technology	RRID: AB_2616028
β-actin	Cell Signaling Technology	RRID: AB_2242334
SOX2	Cell Signaling Technology	RRID: AB_2195767
Normal Rabbit IgG	Cell Signaling Technology	RRID: AB_1031062
Anti-HA	Cell Signaling Technology	RRID: AB_10693385
Bacterial and virus strains		
shSMAD1	Dharmacon (SMART-vector lentiviral human SMAD1 hEF1A-turboGFP shRNA)	N/A
NTC lentivirus	Dharmacon (SMART-vector Non-Targeting Control)	N/A
Plasmid for pCMV3	Sino biological	CV011
EF1A-SOX2 lentivirus	Cellomics Tech	PLV-10013
LV-CMV-SOX2 lentivirus	Cellomics Tech	PLV-10008
Plasmid for shSOX2	Sigma	TRCN355694, TRCN3253
Plasmid for pGL3-SOX2 promoter	Addgene	101761
pHIV-Luc-ZsGreen	Addgene	39196
Adenovirus: pcDNA3-ALK3QD-HA	Miyazono(Imamura et al., 1997)	N/A
Adenovirus: pcDNA3-ALK2QD- HA	Miyazono(Imamura et al., 1997)	N/A
Plasmid for SV40 renilla	Lab Stock	N/A
Chemicals, peptides, and recombinant proteins		
BMP2,4,9,10, TGFβ, Activin	R&D Systems	355-BM, 314-BP, 3209-BP, 2926-BP, 240-B
Luciferin	Goldbio	LUCK
Dorsomorphin	Sigma-Aldrich	p5499
SB431542 hydrate	Sigma-Aldrich	S4317
5-Azacytidine	Sigma-Aldrich	A2385
LDN193189	Sigma-Aldrich	SML0559
ML347	Tocris Bioscience	4945
GSK126	Sooryanarayana Varambally	N/A
MG132	Fisher Scientific	17485
Critical commercial assays		
Mini/Midi prep Kit	Zymo Research	D4036
LIVE/DEAD™ Viability/Cytotoxic kit	Fisher Scientific	L3224
MethylAmp DNA modification kit	Epigentek	P1001
DNeasy Blood & Tissue kit	Qiagen	69504

REAGENT or RESOURCE	SOURCE	IDENTIFIER
Mach4 Universal Detection Kit	BioCare	# M4U534
Background Punisher	BioCare	#BP974
Da Vinci Green Diluent	BioCare	#PD900
3,3′-diaminobenzidine (DAB)	BioCare	#BDB2004
TUNEL kit	ABP Biosciences	A049
PureLink PCR Purification Kit	Invitrogen	#K310002
Alanine Transaminase (ALT) assay kit	Cayman Chemical	700260
Human BMP9 DuoSet ELISA	R&D Systems	DY3209
Human TGF-β1 ELISA	Aushon Biosystems	N/A
Human TGF-β2 ELISA	Aushon Biosystems	N/A
Matrigel	Fischer Scientific	47743-720
SRB salt	Aesar	A14769-14
Lipofectamine RNAimax	ThermoFisher Scientific	13778075
Lipofectamine LTX	ThermoFisher Scientific	15338100
Opti-MEM medium	ThermoFisher Scientific	31985070
Dual Luciferase Assay System	Promega	E1910
Deposited data		
RNA sequencing for PA1 cells	GEO database	GEO: GSE185932
Microarray data for PA1 cells	GEO database	GEO: GSE185924
Experimental models: Cell lines		
PA1	ATCC	CRL-1572
SKOV3	ATCC	HTB-77
HEY	Susan Murphy	N/A
HEK293	ATCC	CRL-1573
OVCAR3	NIH	NCI60 (0507709)
OVCAR4	NIH	NCI60
OVCAR5	NIH	NCI60
M41	Susan Murphy	N/A
IGROV	NIH	N/A
A2780	Susan Murphy	N/A
OVCA420	Susan Murphy	N/A
OVCA433	Susan Murphy	N/A
OVCA429	Susan Murphy	N/A
SKOV3-luc-GFP	This Paper	N/A
PA1-Luc-GFP	This Paper	N/A
SKOV3-CMV-SOX2OE	This Paper	N/A
PA1-EF1a-SOX2OE	This Paper	N/A
p76	Amir Jazaeri	N/A
p211	Amir Jazaeri	N/A
BON-1	Renata Jaskula-Sztul	N/A
H727	ATCC	NCI-H727
A549	ATCC	CRM-CCL-185

REAGENT or RESOURCE	SOURCE	IDENTIFIER
EOC15	Penn State	N/A
AF68	UAB	N/A
Experimental models: Organisms/strains		
NOD/SCID	Jackson Labs	001303
Fox Chase SCID	Charles River	CB17/lcr
Oligonucleotides		
siSMAD3	Ambion	4392420
siSOX2	Ambion	AM16708
siNTC	Ambion	4390843
Primers used for qRT-PCR (see Table S1)	This Paper	N/A
Primers used for Chromatin immunoprecipitation (see Table S2)	This Paper	N/A
Primers used for MS-qPCR (see Table S3)	This Paper	N/A
Software and algorithms		
ImageJ	NIH	https://imagej.net/ImageJ
Prism9	GraphPad	https://www.graphpad.com/scientific-software/prism/
Adobe Illustrator	Adobe	https://www.adobe.com/products/illustrator.html
REACTOME	Reactome Pathway Database	https://reactome.org/
Cell Profiler	Cell Profiler cell image analysis software	www.cellprofiler.org